

2011

**FRACTURE MECHANICS APPROACH  
ON FATIGUE ANALYSIS OF BITUMINOUS  
MATERIAL**

**ALOYSIUS TJAN**

56914 / T - R  
11 - 94

**Perpustakaan  
Universitas Katolik Parahyangan  
Jl. Merdeka 19  
BANDUNG**

625.85

TJA

f

**UNIVERSITAS KATOLIK PARAHYANGAN  
1993**

FRACTURE MECHANICS APPROACH  
ON FATIGUE ANALYSIS OF BITUMINOUS MATERIAL

Aloysius Tjan

I. INTRODUCTION

Flexible pavement has been used as road construction for centuries. And for centuries pavement construction was designed entirely based on experience (empirical) up to the beginning of 20th century. The first attempted to design the pavement on a theoretical approach is made by Burmister in 1943. The first attempted to provide a more "scientific approach" based on the very well documented pavement construction and measured pavement distress with traffic on a regular basis was begun in the late 50's to the early 60's. This well-known field test is the AASHO Road Test. The results from the Road Test are still being used in many countries. The AASHO Road test results have been applied far beyond the limits of the original data (Hall & Elliot, 1992).

The outcome of AASHO (now AASHTO) Road Test findings were used to develop the *Interim Guide for Rigid and Flexible Pavements* published in 1961. The *Interim Guide* was revised in 1972 and 1981. The approach for these manuals were still empirical (AASHO Road Test findings). The most recent revised manual is *AASHTO Guide for Design of Pavement Structures* in 1986. This manual imposes mechanistic-empiric approach

(combination of AASHO Road Test findings and new findings from the recent research publications).

Other agencies such as Shell and Asphalt Institute have implemented this "new" approach (mechanistic-empirical approach) to the pavement design for their manuals in 1978 and 1981 respectively.

Mechanistic design procedures are based on the assumption that a pavement can be modelled as multi-layered elastic or visco-elastic structure on an elastic or visco-elastic foundation. From this model, it is possible to calculate the stress, strain, or deflection due to traffic loading at any point in the pavement structure. However, pavement performance will be influenced by a number of factors which will not be precisely modeled by mechanistic methods. It is necessary to calibrate the models with observations performance. This approach is referred as mechanistic-empirical approach.

The relationship between stresses or strains and the fatigue life of the material can be obtained in the laboratory test. However, the loading condition and temperature in the laboratory are different from the actual pavement. In the laboratory, the test conditions are made simple compared to field conditions. Calibration factor to the laboratory result is used to give "real fatigue life". This relationship is called as a field shift factor. This factor accomodates everything that influence pavement life that has not been taken into account by theory and laboratory test condition.

The major drawback of the procedure is that it may be not applicable to new area (such as different traffic loads and climate condition) that has no previous experience. It is even more difficult to apply it for a new pavement material.

One of the major pavement design criteria is cracking, in addition to rutting. Cracks developed in pavement associated mainly with load from traffic, and to some less extent due to the environment. Mechanistic-empirical approach and elasticity theory is not sufficient to predict the onset of failure. The difficulty is due to the geometry of crack tip. The crack tip is sharp with radius of curvature approaching zero. The local stresses tend to infinity at the crack tip. Since the stresses go to infinity for any loading, the theories of failure can not be applied, and the load required to produce the onset of crack propagation can not be predicted. To treat structure containing cracks, it is necessary to use a method which deals with the singular states of stress at the crack tip, such as fracture mechanics.

The fracture mechanic approach offers a significant improvement to the capability of predicting crack development in a pavement structure. Fracture mechanics is relatively new application for pavement analysis. It was introduced in 1970's. The theory of fracture mechanics itself has been developed since 1960's and the major development of this theory is in the metal (material) engineering.

The process of crack growth (initial cracks, crack propagation) in the pavement structure is reviewed with respect to the fracture mechanics approach. The pavement structure (bituminous layer) is not an elastic but visco-elastic material. Because of rheology the analysis of pavements is more complicated than the traditional linear elastic assumption.

The paper will discuss the fracture mechanics theory, their models for crack development, how they can be applied to pavement material, and also the recent research results with fracture mechanics approach in the pavement area.

## **II FATIGUE TEST**

At the first International Conference on the Structural Design of Asphalt Pavements in 1962, Ann Arbor, Michigan, it was generally accepted that fatigue was a primary cause of cracking (Pell, 1967). There can be little doubt that under traffic loading the layers of flexible pavement structure are subjected to repeated flexing that produce cracking. This conclusion followed the observations made at WASHO and AASHO Road Tests. These developments led to research of fatigue behaviour of bituminous mixture.

The greatest difficulty in interpreting fatigue test results arises because the results are influenced by the method of testing. Fatigue testing of bituminous mixture can be divided into two categories. In controlled stress tests,

the loading produces an alternating stress at a constant amplitude. In controlled strain tests the loading produces an alternating strain or deflection of a constant amplitude.

The results are influenced by the test methods can be clearly explained with Figure 2.1. In controlled stress, the stiffer the mix the longer the life (Fig 2.1a). Fig. 2.1b is the result of sinusoidal controlled stress, replotted in terms of strain and number of loading. The results from different stiffness coincide and indicating that strain is a major criterion of failure.

In controlled strain the result is reversed, the stiffer the mix the lesser the life (Fig. 2.1c). The reason of this is that the mode of failure is different in the two types of test. In the rotating bending (controlled stress machine) the formation of a crack results in an increase in actual stress at the tip of the crack (due to the concentration stress) and this leads to rapid crack propagation, and complete fracture. On the other hand, cracking results in a decrease in stress, hence a slow rate of propagation.

During the test the stiffness of the mix is constant in controlled stress, but at the controlled strain the stiffness reduces with increasing number of load applications at low stiffness. At high stiffness the stiffness changes is negligible (Pell, 1967).

Monismith (1966) as quoted by Pell (1967) concluded that controlled stress define the fatigue behaviour of thick

bituminous layer (4 in or more), while controlled strain define the fatigue behaviour of thin bituminous layer (2 in or less).

In addition to the rotating bending test method, fatigue life can be evaluated with the diametral test and four point bending test.

Diametral fatigue test became popular because of the following reasons (Kim, et.al., 1991):

1. The test is relatively simple,
2. Sample fabrication is easy,
3. The same test configuration has been standardized by ASTM to determine indirect tensile strength and resilient modulus of asphalt concrete (ASTM D4123). The apparatus are shown in Fig. 2.2, 2.3 and 2.4,
4. Failure is initiated in a region of relatively uniform tensile stress, and
5. Stress and strain solutions are readily available.

Repeated haversine load with 0.1 sec. duration and 0.5 sec. rest period are applied until the specimen 'fails'. This is controlled stress test. Horizontal and vertical deformation recorded. Based on their research at 32°F (0°C) and 68°F (20°C) the horizontal deformation increased dramatically after 0.1 in (2.5 mm), and then this value is defined as the failure criteria. The linear relationships log-log scale between

fatigue life and recoverable strain during unloading of every 200th cycle load was found.

Khosla (1991) performed diametral fatigue tests using square wave with 0.1 sec. loading period and 2.9 sec. rest period and a stress level in the range 15 to 50 psi, at 70°F (21°C). The initial strain was measured between 100 and 200 load cycles, and the failure is defined as load reaching 70% of the original load. To adjust the laboratory result to the field condition the Finn's shift factor (13.03) is used.

The recent OECD field test is FORCE Project, with a circular test track at The LCPC Central Laboratory for Roads and Bridges, Nantes in France (OECD, 1991). To get the shift factor, four-point bending controlled stress fatigue test was used. The beam dimension was 450x50x50 mm and loading frequency was of 30 Hz. The fatigue life was determined when the applied load decreases to 50% of the original load. As the result, the shift factor between the laboratory and the field track is between 5.62-6.16.

The effect specimen surface has never been put into consideration in the analysis. However, Harvey, et.al.(1991) shows that there is an effect to result on bituminous parameters as a contribution of specimen surface. In some type of tests, cut surface may significantly affect the measured response of the mixture. In the test with large shear stress components, the measured values of the strength tend to be larger for specimens with cut surfaces. The cut surfaces of



the aggregates rest against the end of plates, effectively resisting rotation of the large particles. This mechanism will produce an effective increase of stiffness modulus, resistance to permanent deformation, and fatigue life. This hypothesis is corroborated by the results of the project compaction study, which show greater modulus, resistance to plastic deformation, and fatigue life for rolling-wheel specimens with cut surfaces, than kneading specimens with uncut surfaces.

The crack propagation in bituminous mix plays an important and complicating role. A considerable amount of crack propagation will have to occur over a wide area before any serious deterioration of the pavement occur.

A criterion to limit the area of cracks appears in the pavement surface can be seen in different current design methods, such as Shell Design Method (1978) and The Ninth Asphalt Institute Thickness Design Manual (MS-1) 1983.

### **III THE ASPHALT INSTITUTE CRACKING PREDICTION**

Extensive research has indicated that fatigue cracking in bituminous mixture can be described by the following relationship:

$$N_f = A (1/\epsilon)^n \quad \dots (3.1)$$

Fatigue cracking models have been developed based on laboratory testing, and in a limited number of cases that

cracks observed in the field correlates with laboratory test result Monismith, et al. (1972) as quoted by Finn, et. al. (1977). Finn, et. al. (1977) proposed a fatigue model that dependent on two analysis:

- 1) Representative fatigue lives from the laboratory.
- 2) Develop a shift factor to provide results compatible with field observations.

The representative laboratory fatigue cracking and repeated loading relationship used by Finn, et. al. (1977) was (constant stress):

$$\log N_f = 14.82 - 3.292 \log (\epsilon/10^{-6}) - 0.854 \log (E^*/10^3) \dots (3.2)$$

Using a bituminous mixtures with characteristics similar to the pavement surface at the AASHO Road Test (Section 315) Finn, et. al., measured the dynamic modulus, at different temperature and loading frequency. For the other pavement layers moduli was estimated from equations in the literature.

Thickness of each pavement layer for every section in AASHO Road Test is available. The moduli of the pavement structure are predicted at the average monthly pavement temperature. Based on the assumption that pavement structure is multi layer elastic, tensile strain due to the traffic loading at the bottom of bituminous layer can determined. The fatigue life for that pavement structure at that particular

temperature is determined by Equation (3.2). The monthly damage was calculated by applying the Miner's hypothesis, as the following:

$$D_i = n_i/N_i \quad \dots (3.3)$$

The cumulative damage in the pavement structure is the summation of damage of each period. Theoretically the number of repeated loading for that pavement structure is achieved when the cumulative damage is equal to one. An example of this procedure for Section 315 of AASHO Road Test is presented in Table 3.1.

If the laboratory result is perfectly related to the field condition, and the pavement damage can be modelled by Miner's hypothesis, the fatigue cracking will occur between March and April. Two criteria was adopted for pavement failure based on the intensity of cracking in the pavement surface that is 10% cracking (lower limit) and 45% Cracking (upper limit).

If the laboratory result is perfectly related to the field condition, and the pavement damage can be modelled by Miner's hypothesis, the fatigue cracking will occur between March and April. Two criteria was adopted for pavement failure based on the intensity of cracking in the pavement surface that is 10% cracking (lower limit) and 45% cracking (upper limit).

On September 1959 there was 3.5% area of pavement with cracks observed, and the cracks on October 1959 is more than 10%. On September the cumulative damage was 13.03. One of the reasons for cumulative damage is higher than 1 is due more loading required for creating a significant number of cracks at the surface. The shift factor for the lower limit is 13.03. With the same procedure for the upper limit, the shift factor is 17.08.

Table 3.1. Cumulative Fatigue Cracking for  
AASHO Road Test Section 315

Month Damage	Year	Monthly damage	Cumulative
November	1958	0.03631	0.03631
December	1958	0.03580	0.07211
January	1959	0.03240	0.10451
February	1959	0.05584	0.16035
March	1959	0.35125	0.51160
April	1959	1.00411	1.51571
Mei	1959	2.12563	3.64134
June	1959	2.50896	6.15031
July	1959	2.74972	8.90003
August	1959	2.43565	11.33568
September	1959	1.69281	13.02849 <sup>1</sup>
October	1959	1.18476	14.21325
November	1959	0.07842	14.29166
December	1959	0.08505	14.37671
January	1960	0.13833	14.51505
February	1960	0.14044	14.65548
March	1960	2.42192	17.07740 <sup>2</sup>

1) Less than 10% cracking

2) More than 45% cracking

The final fatigue life (crack prediction) equation after imposing the shift factor are the followings:

1) For cracks less than 10%

$$\log(N_f) = 15.947 - 3.291 \log(\epsilon/10^{-6}) - 0.854 \log(E^*/10^3) \dots (3.4)$$

2) For cracks more than 45%

$$\log(N_f) = 16.086 - 3.291 \log(\epsilon/10^{-6}) - 0.854 \log(E^*/10^3) \dots (3.5)$$

These equations were used in the development of The Ninth Edition of Asphalt Institute Pavement Thickness Design Manual (MS-1). A similar approach was used for developing the Shell Design Manual.

#### IV FRACTURE MECHANICS APPROACH

There are at least two approaches for design material under tensile stress, i.e., (1) strength of materials approach; and (2) fracture mechanics approach. In the first approach the design has two variables, i.e. applied tensile stress, and tensile strength of the material. It is considered the design to be adequate if the applied tensile stress is less than the tensile strength of the material. On the second approach there are three important variables, i.e., applied tensile stress, flaw size in the material, and fracture toughness. Fracture mechanics quantifies the critical combinations of these variables.

In linear elastic fracture mechanics, material will fracture when sufficient tensile stress applied on the atomic level to break the bonds that hold atoms together. Theoretically the tensile (cohesive) strength of the material is equal to  $E/\pi$ . However, the experimental fracture strength is much lower than this value. As fracture can not occur unless stress at the atomic level exceeds the cohesive strength, thus discrepancy between the actual strength and theoretical strength was due to flaws in the material. The flaws must magnify the stress locally. Westergaard (1939), Sneddon (1948), Irwin (1957), and Williams (1957) were among the first to publish stresses at the vicinity of crack.

The cracks developed under repeated loading condition is fatigue cracking. This is a process of progressive damage leads to failure of the structural system. As a phenomenon complex nature, it involves a localized progressive structural change within the material. This can be divided into three stages (Majidzadeh, 1976):

#### 1. Crack initiation.

During crack initiation, micro cracks are originated at centers of impurities, flaws, and microstructural defects. These centers of strain-incompatibility (when subjected to reversed cyclic strain) are believed to be responsible for the crack initiation process.

## 2. Crack growth.

This process can be divided into Stage I and Stage II crack growth. In Stage I, cracks have microscopic dimensions. In Stage II, cracks have macroscopic dimensions and it can be identified and measured in the test or in the existing structure. It also precedes catastrophic failure. The distinction between these stages is not very obvious and depends on the equipments used. The Stage II crack growth is commonly referred to as crack propagation.

## 3. Terminal state of fracture.

The occurrence of these processes in a material system results in a gradual weakening of the structural component.

The process of crack propagation and the terminal state of fracture have been treated by numerous theories. The introduction of fracture mechanics principles into the analysis of fatigue of material systems has provided an analytical method of classifying the crack severity, and a rational scheme for the life expectancy calculations of structural systems.

There are two approaches to analyse the fracture:

### 1. The Energy Approach

The energy approach states that crack extension (i.e. fracture) occurs when the energy available for the crack growth is sufficient to overcome the resistance of the

material (Anderson, 1991). The material resistance may include the surface energy, plastic work, or other type of energy dissipation associated with a propagating crack.

According to Irwin (1956) as quoted by Anderson (1991) energy release rate (as a driving force),  $G$ , in an infinite plate is a function of remote tensile stress, crack length and Young's Modulus as the following (Fig. 4.1):

$$G = \pi (\sigma^2) a/E \quad \dots (4.1)$$

At the moment of fracture occurs,  $G = G_c$ .  $G_c$  is the critical energy release rate, which is the measure of fracture toughness (as material's resistance to fracture). It is assumed that  $G_c$  is independent of the size and geometry of the cracked body, so fracture toughness measurement on specimen in the laboratory can be applied to the structure.

## 2. The Stress Intensity Approach

The stresses near the tip of crack in an elastic material in the plane stress is proportional to  $K_I$  (stress intensity factor). Stress intensity factor,  $K_I$  (as a driving force) is given as:

$$K_I = \sigma (\pi a)^{0.5} \quad \dots (4.2)$$



Crack occurs when  $K_I = K_{Ic}$ .  $K_{Ic}$  is critical stress intensity, as a measure of material resistance.  $K_{Ic}$  is also assumed to be independent of size of the material.

The relation between  $G$  from energy approach and  $K_I$  from stress intensity approach is:

$$G = K_{I2}^2/E \quad \dots (4.3)$$

The same relationship holds for  $G_c$  and  $K_{Ic}$ . Thus energy and stress intensity approaches are essentially equivalent for linear elastic materials.

In a mechanistic approach, it is postulated that crack growth is a consequence of the changing crack tip profile. During a cycling deformation, a crack will have a phenomenon of blunting and resharping. In tensile loading cycles, the crack tip tends to open first and then blunted as the plastic zone forms and spreads ahead of the crack tip. During the unloading cycle, the elastic contraction of the material surrounding the crack imposes a residual compressive stress on the plastically-deformed material at the crack tip. This reduces ductility and resharpens the crack which generates the growth of the crack in the next loading cycle. This process leads to slow crack growth until the crack reaches a critical size, where unstable fracture occurs. The stress intensity at the crack tip affecting the rate of crack growth. The stress

intensity is determined by stress and strain amplitude and the defect size.

Fracture type due to the loading mode can be divided into 3 mode. They are as the following (Fig. 7.2):

1. Mode I loading is when the principal load is applied normal to the crack plane and tends to open the crack.
2. Mode II loading is when in-plane shear loading happens and tends to slide one crack face with respect to the other.
3. Mode III loading refers to out-of-plane shear.

A crack body can be loaded in any one of these modes or a combination of those three.

The stress field in the crack tip neighbourhood controls the subcritical crack growth rate. Factor describing the stress field in the neighbourhood of the crack tip is the stress intensity factor. Fatigue models that have the stress intensity factor gained wide acceptability.

The stress at the crack tip is a function of stress intensity,  $K$ , and the loading mode. Stress equations for each mode can be seen in Table 4.1. Stress intensity solutions are related to geometry and loading mode.

$$K_{(I, II \text{ or } III)} = C \sigma (\pi a)^{0.5} \quad \dots (4.4)$$

Equation for  $K_I$  for specimen tested in the laboratory depends test method. Table 4.2 describes the different equations for

each type of testing. In the table there is only  $K_I$  because in most cases mode I is the major problem to crack.

Wells (1961) attempts to measure  $K_{Ic}$  (critical stress (intensity) of steels, and he founds that these materials were too tough to be characterized by linear elastic fracture mechanics. Wells noticed that crack faces had moved apart prior to fracture, plastic deformation blunted an initially sharp crack. This observation led Wells to propose the opening at the crack tip as a measure of fracture toughness (CTOD=Crack Tip Opening Displacement).

$$\delta = K_I^2 / (m \sigma_{ys} E') = G / (m \sigma_{ys}) \quad \dots (4.5)$$

For brittle materials,  $K_{Ic}$  is the criteria for stress intensity to promote fracture. This criteria is not applicable to material which has ductile or creep characteristic. The stress intensity criteria to fracture for ductile material is  $J_c$  and for material with creep characteristic is  $C^*$  (Line Integral). These parameters are powerful tool to characterize the fracture process in a more general term, because they can be used for the brittle material too.

## V FATIGUE CRACK PROPAGATION

So far the material discussed has dealt with static or monotonic loading of cracked body. In early 1960s, Paris, et al. (1961) demonstrated that fracture mechanics is a useful

tool to characterizing fatigue crack growth. Since then, the application of fracture mechanics to fatigue problems has become almost routine.

Consider a growing crack in the presence of a constant amplitude cyclic stress intensity. A cyclic plastic zone forms at the crack tip, and the growing crack leaves behind a plastic wake. If the plastic zone is sufficiently small that it is embedded within an elastic singularity zone, the conditions at the crack tip are uniquely defined by the  $K$  value, and the crack growth rate is characterized by  $K_{min}$  and  $K_{max}$ , as the following form:

$$da/dN = f_1(\delta, K, R) \quad \dots (5.1)$$

By integrating the equation from initial crack length  $a_0$  to final crack length  $a_f$ , the estimate fatigue life can be obtained.

Excessive plasticity during fatigue can violate similitude, since  $K$  no longer characterizes the crack tip conditions. In this case Lambert, et al. (1988) applied the  $J$  integral to fatigue accompanied by large scale yielding.

$$da/dN = f_2(\delta, J, R) \quad \dots (5.2)$$

This equation is in more general form because it is still valid in the case of constant amplitude fatigue in small

yielding. Experimental data from Lambert (1988) shows that delta J correlates crack growth data reasonably well in certain cases. Tanaka (1989) has found that CTOD may also be suitable parameter for fatigue under elastic-plastic conditions.

## VI JUSTIFICATION OF APPLICATION FRACTURE MECHANICS IN PAVEMENT

### 1. Applicability of Fracture Mechanics to Pavement Materials.

Due to the heterogenous nature of common bituminous mixture, initially a relatively uniform mix of sand-asphalt was selected for testing in the laboratory (Majidzadeh, et.al., 1991). The results obtained indicated that the rate of crack propagation,  $da/dN$  could be represented by Paris's crack growth law:

$$da/dN = A K^n \quad \dots (6.1)$$

Subsequent research included bituminous mixture containing aggregates which were used in the surface mixes by the Ohio Department of Transportation. Researchers observed that Equation (6.1) was still valid for heterogenous mixes.

### 2. Applicability of Fracture Mechanics to Analyse Pavements.

Pavement structures are affected by several variables, such as support condition, traffic loading, environmental condition and structural geometry.

Two different supports condition were used for the laboratory tests (Majidzadeh, et.al.,1991), i.e. simple support beam, and specimen on elastic foundation. Dimension of the beam is 3 in x 2 in x 24 in (widthx depth x length), and dimension of the slab is 44 inches in diameter and 1.5 inches thick. The results indicate a significant effect of support conditions on the rate of cracking, both on parameter A and n (Figure 6.1). The rate of cracking for simple support beam is the highest, and good foundation gives less rate of cracking.

For the monotonic loading of constant amplitude on an elastic foundation, the rate of crack of propagation is proportional to stress intensity factor. Conversely crack propagation is independent of:

- load level, from 20, 30 and 40 lbs (Figure 6.2)
- geometry of the specimen i.e., beam and slab (Figure 2.3)
- rest period for both beam and slab. In the test, half sine load (0.1 sec) is used. The variation of the rest periods is 0, 0.4, 0.8 sec. (Fig 6.4).

There is a significant effect of load sequence on the rate of cracking in beam specimens which is shown in Fig. 6.5. It happens for either beam or slab specimens.

The Equation 6.1 is still valid for 2 different temperatures (41°F and 90°F) that has been observed on slab specimens (Fig. 6.6 and Fig. 6.7). At higher temperature, A will be higher, while n is constant (=4), it means that at higher temperature the rate of cracking is higher.

Parameters A and n will decrease as dynamic modulus of mixture increases. Mixture with a higher dynamic modulus the rate of cracking will be lower.

## VII LABORATORY RESULT ON FRACTURE PROPERTIES

To determine the value  $K_{Ic}$  from the laboratory test for a particular specimen geometry, calibration of  $K_{Ic}$  should be performed. Monismith, et al. (1971) have done  $K_{Ic}$  calibration. There are two type of specimen used in their tests.

1. The specimen size of 1.5 in x 2.0 in x 15.0 (width x depth x length) prismatic beam with single-edge-notched. The loading is continuous four-point bending loading.
2. The specimen size of 1.5 in x 1.5 in x 4.5 in (width x breadth x height) with single-edge-notched. The loading is continuous tension loading.

The notch for both type of specimens was cut with a V-tipped diamond saw having a tip radius of 0.001 in. The mix designations are shown in Table 7.1.

The stress intensity factor for specimen with four-point bending is calculated with the following equations:

$$K_{Ic} = f(a/h) \sqrt{6 M_c (a)^{0.5} / (b h^2)} \quad \dots (7.1)$$

$$K_{Ic} = g(a/h) \sqrt{6 M_c / (h - a)^{1.5}} \quad \dots (7.2)$$

$$f(a/h) = 1.99 - 2.47(a/h) + 12.97(a/h)^2 - 23.17(a/h)^3 + 24.80(a/h)^4 \quad \dots (7.3)$$

Table 7.2. Calibration Function  $g(a/h)$  as function of  $(a/h)$

$(a/h)$	$g(a/h)$
0.05	0.36
0.1	0.49
0.2	0.6
0.3	0.66
0.4	0.69
0.5	0.72
$\geq 0.6$	0.73

$K_{Ic}$  obtained from these equations were essentially the same. Using the first equation, the revised calibration function is shown in Fig. 7.1 and the expression has the following form:

$$f(a/h) = 2.17 - 4.24(a/h) + 20.53(a/h)^2 - 35.21(a/h)^3 + 29.51(a/h)^4 \quad \dots (7.4)$$

For single-edge-notched tension specimens, the calibration of  $f(a/w)$  is the following (Fig. 7.2):

$$K_{Ic} = f(a/w) \sqrt{P_c (a)^{0.5} / (b w)} \quad \dots (7.5)$$

$$f(a/w) = 1.99 - 0.41(a/w) + 18.70(a/w)^2 - 38.48(a/w)^3 + 53.85(a/w)^4 \quad \dots (7.6)$$



The results (Monismith, 1971) of laboratory test with different mix variable on  $K_{Ic}$ , are as the following:

1. Asphalt content (Fig. 7.3). At cold temperature (-20°F and 10°F with tension tests and -20°F with bending tests)  $K_{Ic}$  increased with asphalt content, but  $K_{Ic}$  decreased at 40°F (tension tests). It may be attributed in part to plastic flow which in turn induces a blunting effect at the crack tip.
2. Asphalt type (Fig. 7.4 and 7.5). At -20°F  $K_{Ic}$  [psi in<sup>0.5</sup>] corresponded to a value of 100 of the penetration.
3. Aggregate gradation (Fig. 7.6 and 7.7). There is an "optimum" temperature for each gradation that gives maximum  $K_{Ic}$ .
4. Air void (Fig. 7.8). Higher  $K_{Ic}$  will be obtained at lower air void.
5. Aging (Fig. 7.9 and 7.10). Aged mix will have higher  $K_{Ic}$ .
6. Mineral filler (Fig. 7.11). The result is similar to the effect of gradation.

#### VIII PREDICTION OF FATIGUE LIFE FROM FRACTURE DATA

A quantitative relationship for crack growth utilizing the stress intensity factor may be formulated from Paris's crack growth law, as Equation 6.1.

Predicting fatigue life is assuming that it is within a significant portion of stable crack growth between initial crack length  $a_0$  and critical crack length  $a_c$ . Fatigue life is determined when  $K_I$  equal to  $K_{Ic}$ .

The incremental growth of a crack may be expressed as an average rate:

$$(\delta a / \delta N) = 0.5 ([A K^n]_{(a)} + [A K^n]_{(a + \delta a)}) \quad \dots (8.1)$$

The number of load repetition resulting in an increment of crack growth  $\delta a$  is:

$$\delta N = (2 \delta a) / ([A K^n]_{(a)} + [A K^n]_{(a + \delta a)}) \quad \dots (8.2)$$

$$\delta N = (\delta a) / [A K^n]_{(a)} \quad \dots (8.3)$$

By integrating Equation 8.3 up to the critical crack length, one can get the value of fatigue life, N.

The main key to this prediction is the relationship between  $K_I$  and  $da/dN$ . The procedure to get this relationship is as the following:

a). Deflection Compliance

Deflections are measured for a combination of different load levels, and notch depths. From these data, deflection compliance, D, can be obtained from the following equation.

$$D = y b/P \quad \dots (8.4)$$

The normalized deflection compliance is the ratio of deflection compliance on specimen with a certain value of  $a/h$  to deflection compliance on specimen with  $a/h=0$ . The

relationship between normalized deflection compliance with  $a/h$  is shown in Fig. 8.1.

b). Crack Compliance

Crack Tip Opening Displacement (CTOD) is directly related to notch depth and to fracture characteristics of material ( $K_I$ ).

The value of CTOD can be expressed as follows:

$$V = (8 \epsilon_y a/\pi) \ln \sec (\pi \sigma/2 \sigma_y) \quad \dots (8.5)$$

Using a series expansion for the  $(\ln \sec)$  expression and using only the first term,

$$V = \pi \sigma^2 a/(E \sigma_y) \quad \dots (8.6)$$

It can also be seen that CTOD is dependent upon  $K_{I2}$ .

$$V = (1 - \nu^2)/E (K_I^2/\sigma_y) \quad \dots (8.7)$$

CTOD are measured for a combination of different load levels, and notch depths. From these data, crack compliance,  $C$ , can be obtained in a similar manner to that of deflection compliance.

$$C = V b/P \quad \dots (8.8)$$

The normalized crack compliance is the the ratio of crack compliance on specimen with a certain value of  $a/h$  to crack compliance on specimen with  $a/h=0$ . The relationship between normalized deflection compliance with  $a/h$  is shown in Fig. 8.2.

c). Repeated loading test

The typical result of the repeated loading from a specimen is shown in Fig. 8.3. If the deflection is measured during the test, the normalized deflection compliance is used to develop Fig. 8.4. If the crack deflection is measured during the test, the normalized crack deflection is used. The final result in the form of graph such as in Fig. 8.4 is the relationship between number of loading (cycles) to  $a/h$ .

d). Relationship between  $K_I$  and  $da/dN$

$da/dN$  is the slope in the final relationship from Fig. 8.4. By using Equation 7.4, one can develop the relationship between  $K_I$  and  $da/dN$  such as shown in Fig. 8.5, and the relationship is the following:

$$(da/dN) = 7.9 (10)^{-17} K_I^{3.8} \quad \dots (8.7)$$

## IX DESIGN PROCEDURE BASED ON FRACTURE MECHANICS

1. The temperatures should be selected as the anticipated temperatures for the material during the service.

2. Develop a relationship of  $K_I$  and  $a/h$  for a particular geometric. This relationship will be use only for the tests with the same geometric.
3. Find out the  $K_{Ic}$  value for the mixture.
4. Find out relationship of normalized compliance- $a/h$  such as deflection, or CTOD. It depends on which measurement will be used for the whole tests.
5. Test the mixture with repeated loading for a various initial notch depth. Record the relationship between deflection or CTOD and number of repeated loading, and develop the relationship between normalized compliance and repeated loading.
6. By using the relationship of normalized compliance- $a/h$ , one can transform normalized compliance-repeated loading to  $a/h$ -repeated loading.
7. Find out the  $K_I-da/dN$ , by utilizing  $K_I-a/h$  and the slope of  $a/h-N$  curve.
8. By utilizing this final relationship ( $K_I-da/dN$ ), one can calculate the number of repeated loading for a particular crack increment.
9. Repeat the calculation until  $K_{Ic}$  is achieved. The summation the number of repeated loading up to  $K_{Ic}$  is the fatigue life.

An example of fatigue life calculation with fracture mechanics approach is presented in the Table 8.1.

Table 8.1 Example of Fatigue Life Calculation

a (1)	$\delta a$ (2)	$\underline{a}$ (3)	$\underline{a}/h$ (4)	$f(\underline{a}/h)$ (5)	$K_I$ (6)	(7)	(8)	$\delta N$ (9)	$\Sigma N$ (10)
0.1									
	0.1	0.15	0.075	1.953	302	0.61	164.0	164.0	
0.2									164.0
	0.1	0.25	0.125	1.899	380	1.58	63.3	63.3	
0.3									227.3
	0.1	0.35	0.175	1.895	448	2.85	35.1	35.1	
0.4									262.4
	0.1	0.45	0.225	1.929	518	5.10	19.6	19.6	
0.5									282.0
	0.1	0.55	0.275	1.993	591	8.94	11.2	11.2	
0.6									293.2
	0.1	0.65	0.325	2.081	671	16.40	6.1	6.1	
0.7									299.3
	0.1	0.75	0.375	2.193	760	27.50	3.64	3.6	
0.8									302.9
	0.1	0.85	0.425	2.336	862	42.50	2.35	2.4	
0.9		0.90	0.450	2.420	900=K <sub>IC</sub>				305.3

- (1), (2), (3) [in]
- (4) = (3)/2
- (5) = Eqn 7.4
- (6) = Eqn 7.1 [psi (in<sup>0.5</sup>)]
- (7) = da/dN [\*10<sup>-6</sup>]
- (8) = dN/da [\*10<sup>4</sup>]
- (9) = (8) \* (2) [\*10<sup>3</sup>]
- (10) [\*10<sup>3</sup>]

**X CONCLUSIONS**

In the mechanistic-empirical approach, it is still not clear which the type of failure that governs in the pavement, either control stress or control strain. This imposes difficulties of determining the model of fatigue testing in the laboratory. The most common short cut to overcome this problem is applying shift factor as a calibration factor from the laboratory result to observed pavement condition. This procedure is still used for the latest reseach by OECD (1991).

With this approach the detail of how the cracks initiate, and propagate is still not perfectly modelled and understood. As the crack is one of the criteria in pavement design, it is very important to understand how it develops due to the traffic loading.

Fracture mechanics improves the ability to predict how crack develops. From the laboratory results,  $K_I$ - $da/dN$  is affected by temperature, sequence of loading, and modulus of subgrade reaction ( $k$ ). In addition to  $K_I$ , depends on age of pavement. Because the pavement structure exposes to a great variation on those parameters, during the service life, it is still difficult to accommodate the changes in pavement life prediction. Miner's hypothesis can not be used here because sequence of loading effect the  $K_I$ .

The above example for fatigue life calculation is made by assuming that parameters that effect the material is constant during the service life.

The current discussion deals the bituminous mix as a linear elastic material, instead of visco-elastic material. The process of the design will become more complicated to accommodate these properties to the fracture mechanics approach.

## REFERENCES

Anderson, T.L. (1991), *Fracture Mechanics, Fundamental and Applications*, CRC Press, Boca Raton, Florida.

Finn, F., C. Saraf, R. Kulkarni, K. Nair, W. Smith and A. Abdullah (1977), 'The Use of Distress Prediction Subsystems for The Design of Pavement Structures', *Proceedings on the Third International Conference of Structural Design of Asphalt Pavements*.

Hall, K.D. and R.P. Elliot (1992), 'ROADHOG-A Flexible Pavement Overlay Design Procedure', *Transportation Research Board, TRR 1374*, Transportation Research Board, Washington, DC.

Harvey, J., J.B. Sousa, J.A. Deacon, and C.L. Monismith (1991), 'Effect of Sample Preparation and Air-void Measurement on Asphalt Concrete Properties', *Transportation Research Record, No. 1317*, Transportation Research Board, Washington, DC.

Inglis, C.E. (1913), 'Stresses in a Plate Due to the Presence of Cracks and Sharp Corners', *Transactions of the Institute of Naval Architects, Vol. 55*.

Irwin, G.R. (1957), 'Analysis of Stresses and Strains near the End of a Crack Traversing a Plate', *Journal of Applied Mechanics, Vol. 24*.

Kim, Y.R., N.P. Khosla, and N. Kim (1991), 'Effect of Temperature and Mixing Variables on Fatigue Life Predicted by Diametral Fatigue Testing', *Transportation Research Record, No. 1317*, Transportation Research Board, Washington, DC.

Khosla (1991), 'Effect of the Use of Modifiers on Performance of Asphaltic Pavements', *Transportation Research Record, No. 1317*, Transportation Research Board, Washington, DC.

Lambert, Y., P. Sailard and C. Bathias (1988), 'Application of the J Concept to Fatigue Growth in Large-Scale Yielding', *ASTM STP 969*.

Majidzadeh, et. al. (1976), 'Evaluation of Improved Mixture Formulations, and the Effect of Temperature Conditions on Fatigue Models', *Application of Fracture Mechanics for Improved Design of Bituminous Concrete, Vol. 2*, FHWA, Report No. FHWA-RD-76-92, Washington, DC.

Majidzadeh, K, C.L. Saraf, S. Mesarovic and G.J. Ilves (1991), 'State of the Art Review of Rutting and Cracking in



Pavements', *Proceedings Unified Airport Pavement Design and Analysis Concepts Workshops*, DOT/FAA/RD-92/17.

Monismith, C.L. (1966), 'Fatigue of Asphalt Paving Mixtures', *Proceedings on First Annual Street and Highway Conference*, Nevada.

Monismith, C.L., R.G Hicks and Y.M. Salam (1971), *Basic Properties of Pavement Components*, FHWA Report RD-72-19.

Monismith, C.L., J.A. Epps, D.A. Kasianchuk, and D.B. McLean (1972), 'Asphalt Mixture Behaviour in Repeated Flexure', Institute of Transportation and Traffic Engineering, Report No. TE 70-5, University of California, Berkeley.

OECD (1991), *OECD Full-Scale Pavement Test*, Organization for Economic Co-operation and Development

Paris, P.C., M.P. Gomez and W.P. Anderson (1961), 'A Rational Analytic Theory of Fatigue', *The Trend in Engineering*, Vol. 13.

Pell, P.S. (1967), 'Fatigue of Asphalt Pavement Mixes', *Proceedings on the 2nd International Conference of Structural Design of Asphalt Pavements*.

Sneddon, I.N. (1946), 'The Distribution of Stress in the Neighbourhood of a Crack in an Elastic Solid', *Proceedings Royal Society of London*, Vol. A-187.

Tanaka, K. (1989), 'Mechanics and Micromechanics of Fatigue Crack Propagation', *ASTM STP 1020*.

Westergaard, H.M. (1939), 'Bearing Pressures and Cracks', *Journal of Applied Mechanics*, Vol. 6.

Wells, A.A. (1961), 'Unstable Crack Propagation in Metals: Cleavage and Fast Fracture', *Proceedings of the Crack Propagation Symposium*, Vol. 1, Paper 84, Cranfield, UK.

Williams, M.L. (1957), 'On the Stress Distribution at the Base of a Stationary Crack', *Journal of Applied Mechanics*, Vol. 24.

## LIST OF NOTATIONS

$a$  = crack dimension, or notch depth, or half of crack length

$\bar{a}$  = average crack length for a given increment

$b$  = beam width, or breadth of specimen

$da/dN$  = crack growth per cycle

$f(a/h)$  = calibration function given by fourth degree polynomial

$f(a/w)$  = calibration function (Fig. 7.1)

$g(a/h)$  = calibration function is given in the Table 7.2

$h$  = beam height

$k$  = modulus of subgrade (foundation) reaction

$n_i$  = number of applications applied during period  $i$

$m$  = constant = 1.0 for plane stress; and 2.0 for plane strain

$n$  = constant (experimentally determined)

$w$  = width of specimen

$V$  = CTOD

$y$  = beam center deflection

$A$  = constant (experimentally determined)

$C$  = constant and depends on geometry and loading mode

$C$  = crack compliance

$D$  = compliance

$D_i$  = damage during period- $i$

$E^*$  = complex modulus; [psi]

$E'$  =  $E$  for plane stress =  $E/(1-\nu^2)$  for plane strain

$E$  = Young's Modulus

F = force

G = energy release rate (per crack increament)

J = compliance (= elastic deformation/F)

K = stress intensity

$K_I$  = stress intensity mode I

$K_{Ic}$  = critical stress intensity factor (fracture toughness)

$M_c$  = critical moment

$N_i$  = fatigue life for condition-i

$N_f$  = number of load repetitions to failure

P = applied load

$P_c$  = critical load

$R = K_{min}/K_{max}$

$\delta$  = crack opening

$\delta K = K_{max} - K_{min}$

$\delta J$  = contour integral for cyclic loading

$\sigma_y$  = yield stress

$\epsilon_y = \sigma_y/E$

$\sigma$  = remote uniform stress (applied load)

$\sigma_{ys}$  = uniaxial yield strength

$\epsilon$  = initial tensile strain

$\nu$  = Poisson's ratio

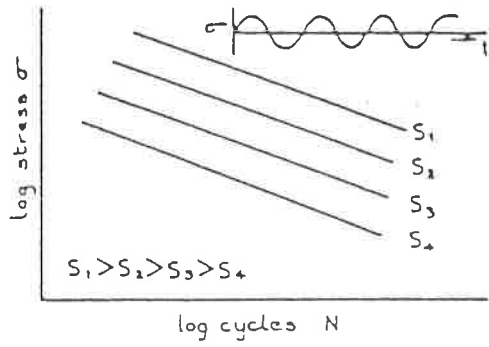


Fig. 2.1a Controlled Stress Fatigue Test at Different Stiffnesses, Stress vs N

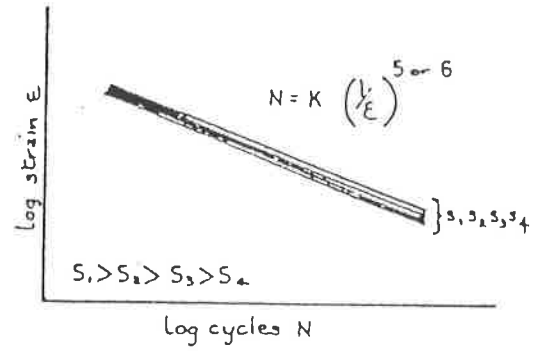


Fig. 2.1b Controlled Stress Fatigue Test, Strain vs N

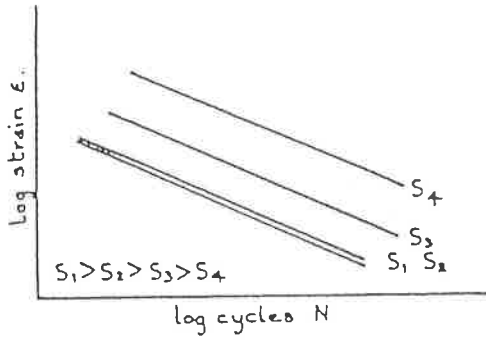


Fig. 2.1c Controlled Strain Fatigue Test at Different Stiffnesses, Strain vs N

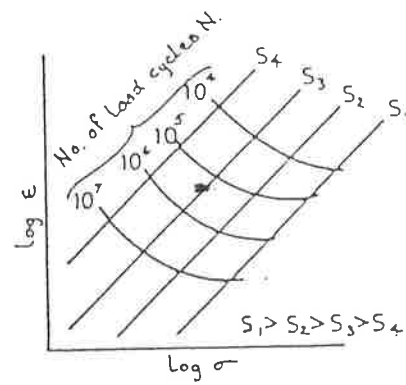


Fig. 2.1d Fatigue Results at Different Stiffnesses Strain vs Stress

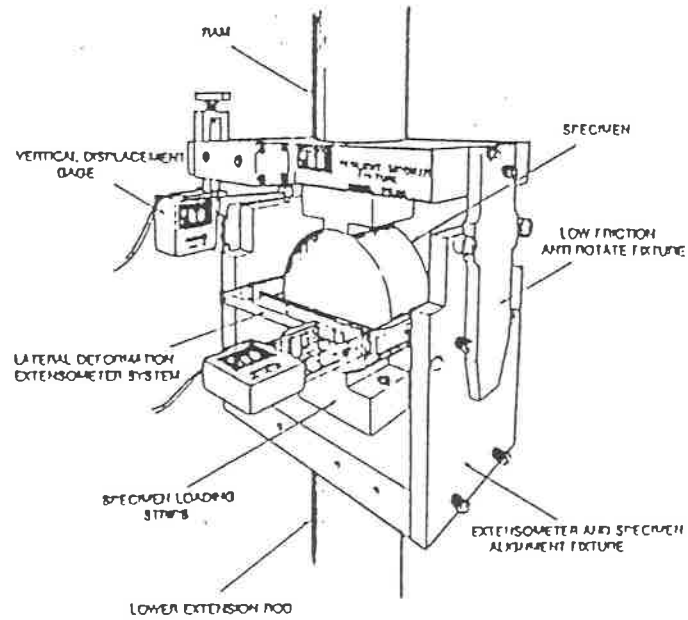


Fig.2.2 Diametral Fatigue Testing Fixture and Extensometer

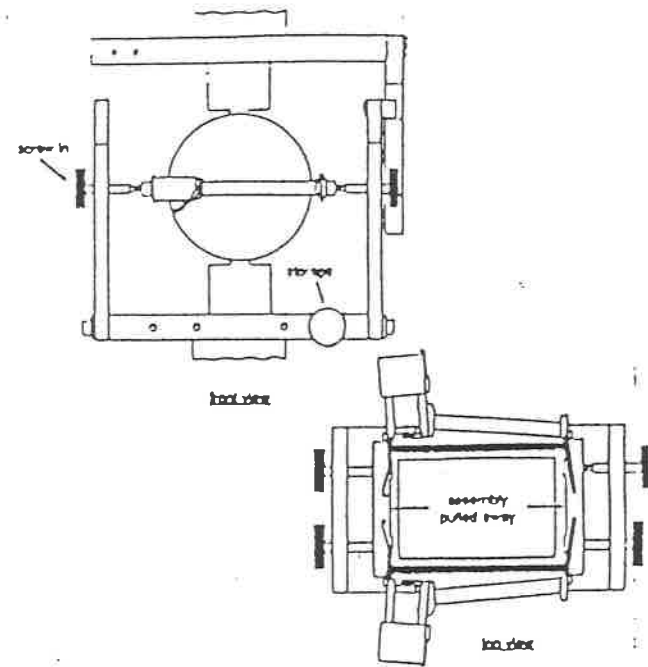


Fig.2.3 Positioning of Side Brackets Using Thumbscrews

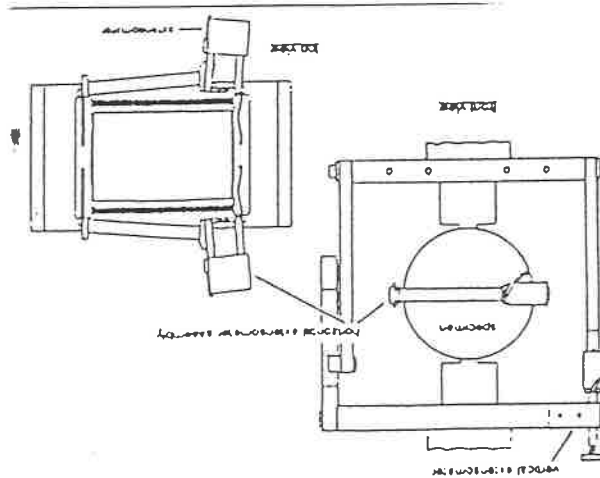


Fig.2.4 Setup Ready for Testing with spring-loaded Extensometer

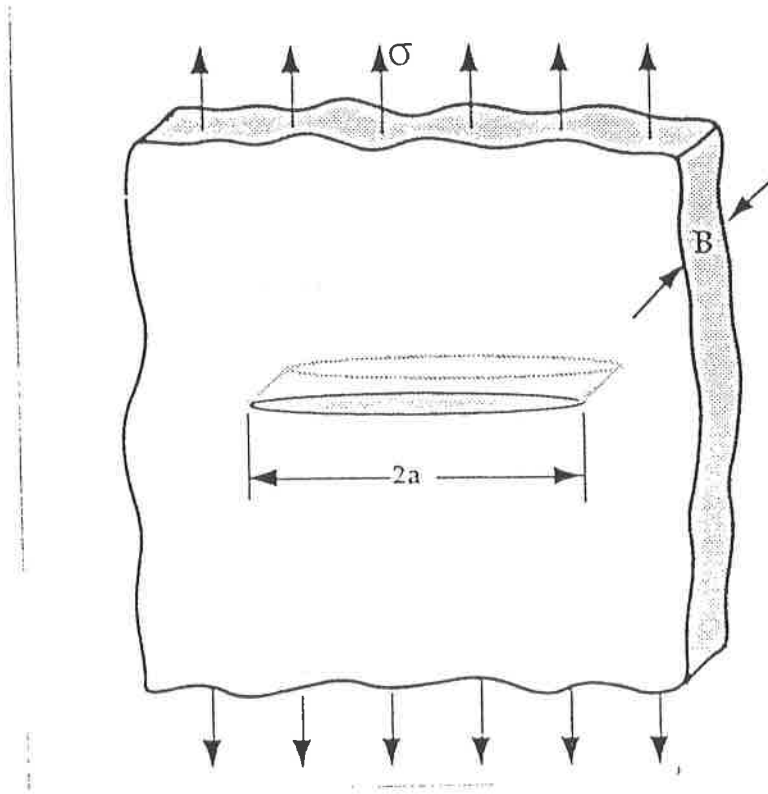


Fig. 4.1 An Infinite Plate Subject to a Remote Tensile Stress

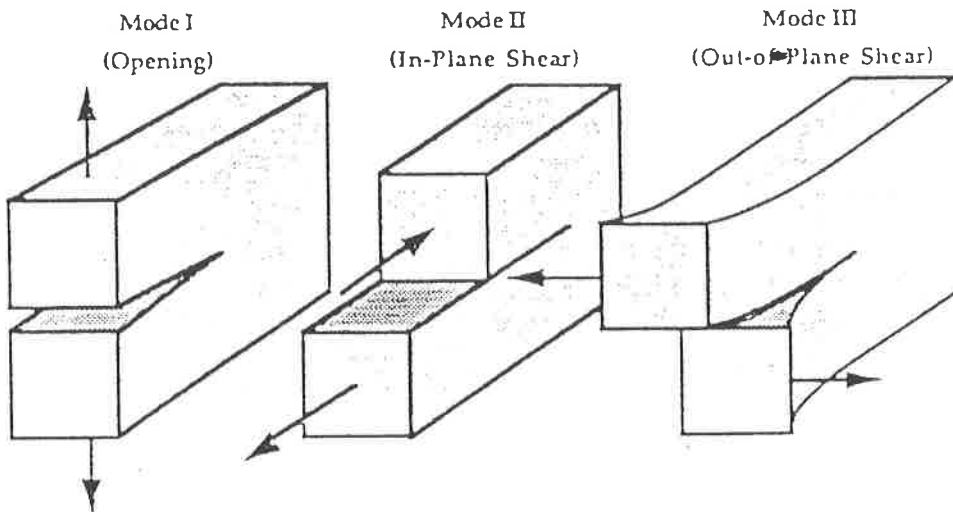


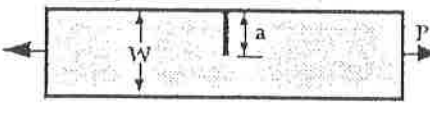
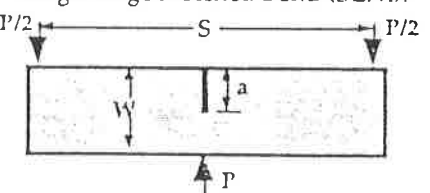
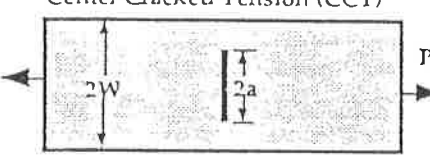
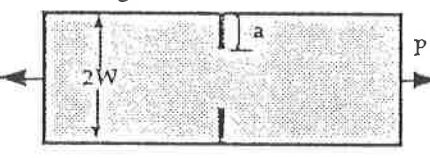
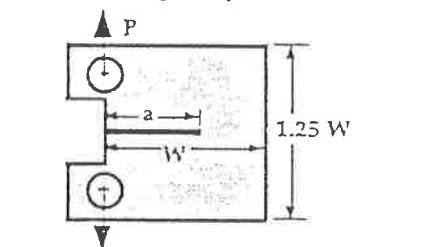
Fig. 4.2 Three Mode of Loadings Applied to a Crack

Table 4.1 Stress Field at Crack Tip  
for Mode I, II and III

	Mode I	Mode II	Mode III
$\sigma_{xx}$	$\frac{K_I}{\sqrt{2\pi r}} \cos\left(\frac{\theta}{2}\right) \left[ 1 - \sin\left(\frac{\theta}{2}\right) \sin\left(\frac{3\theta}{2}\right) \right]$	$\frac{K_{II}}{\sqrt{2\pi r}} \sin\left(\frac{\theta}{2}\right) \left[ 2 + \cos\left(\frac{\theta}{2}\right) \cos\left(\frac{3\theta}{2}\right) \right]$	$\tau_{xz} = -\frac{K_{III}}{\sqrt{2\pi r}} \sin\left(\frac{\theta}{2}\right)$
$\sigma_{yy}$	$\frac{K_I}{\sqrt{2\pi r}} \cos\left(\frac{\theta}{2}\right) \left[ 1 + \sin\left(\frac{\theta}{2}\right) \sin\left(\frac{3\theta}{2}\right) \right]$	$\frac{K_{II}}{\sqrt{2\pi r}} \sin\left(\frac{\theta}{2}\right) \cos\left(\frac{\theta}{2}\right) \cos\left(\frac{3\theta}{2}\right)$	$\tau_{yz} = \frac{K_{III}}{\sqrt{2\pi r}} \cos\left(\frac{\theta}{2}\right)$
$\tau_{xy}$	$\frac{K_I}{\sqrt{2\pi r}} \cos\left(\frac{\theta}{2}\right) \sin\left(\frac{\theta}{2}\right) \cos\left(\frac{3\theta}{2}\right)$	$\frac{K_{II}}{\sqrt{2\pi r}} \cos\left(\frac{\theta}{2}\right) \left[ 1 - \sin\left(\frac{\theta}{2}\right) \sin\left(\frac{3\theta}{2}\right) \right]$	$u_z = \frac{K_{III}}{\mu} \sqrt{\frac{r}{2\pi}} \sin\left(\frac{\theta}{2}\right)$
$\sigma_{zz}$	0 (Plane Stress) $\nu (\sigma_{xx} + \sigma_{yy})$ (Plane Strain)	0 (Plane Stress) $\nu (\sigma_{xx} + \sigma_{yy})$ (Plane Strain)	
$\tau_{xz}, \tau_{yz}$	0	0	

$\nu$  is Poisson's ratio.

Table 4.2  $K_I$  Solution for Common Test Specimens

GEOMETRY	$f(a/W)^*$
<p>Single Edge Notched Tension (SENT)</p> 	$\frac{\sqrt{2 \tan \frac{\pi a}{2W}}}{\cos \frac{\pi a}{2W}} \left[ 0.752 - 2.02 \left( \frac{a}{W} \right) - 0.57 \left( 1 - \sin \frac{\pi a}{2W} \right)^3 \right]$
<p>Single Edge Notched Bend (SENB)</p> 	$\frac{3 \frac{S}{W} \sqrt{\frac{a}{W}}}{2 \left( 1 + 2 \frac{a}{W} \right) \left( 1 - \frac{a}{W} \right)^{3/2}} \left[ 1.99 - \frac{a}{W} \left( 1 - \frac{a}{W} \right) \left( 2.15 - 3.93 \left( \frac{a}{W} \right) + 2.7 \left( \frac{a}{W} \right)^2 \right) \right]$
<p>Center Cracked Tension (CCT)</p> 	$\sqrt{\frac{\pi a}{4W} \sec \frac{\pi a}{2W}} \left[ 1 - 0.025 \left( \frac{a}{W} \right)^2 - 0.06 \left( \frac{a}{W} \right)^4 \right]$
<p>Double Edge Notched Tension (DENT)</p> 	$\frac{\sqrt{\frac{\pi a}{2W}}}{\sqrt{1 - \frac{a}{W}}} \left[ 1.122 - 0.561 \left( \frac{a}{W} \right) - 0.205 \left( \frac{a}{W} \right)^2 - 0.471 \left( \frac{a}{W} \right)^3 + 0.190 \left( \frac{a}{W} \right)^4 \right]$
<p>Compact Specimen</p> 	$\frac{2 + \frac{a}{W}}{\left( 1 - \frac{a}{W} \right)^{3/2}} \left[ 0.888 - 4.64 \left( \frac{a}{W} \right) - 13.32 \left( \frac{a}{W} \right)^2 - 14.72 \left( \frac{a}{W} \right)^3 - 5.60 \left( \frac{a}{W} \right)^4 \right]$

\* $K_I = \frac{P}{B \sqrt{W}} f(a/W)$  where B is the specimen thickness.



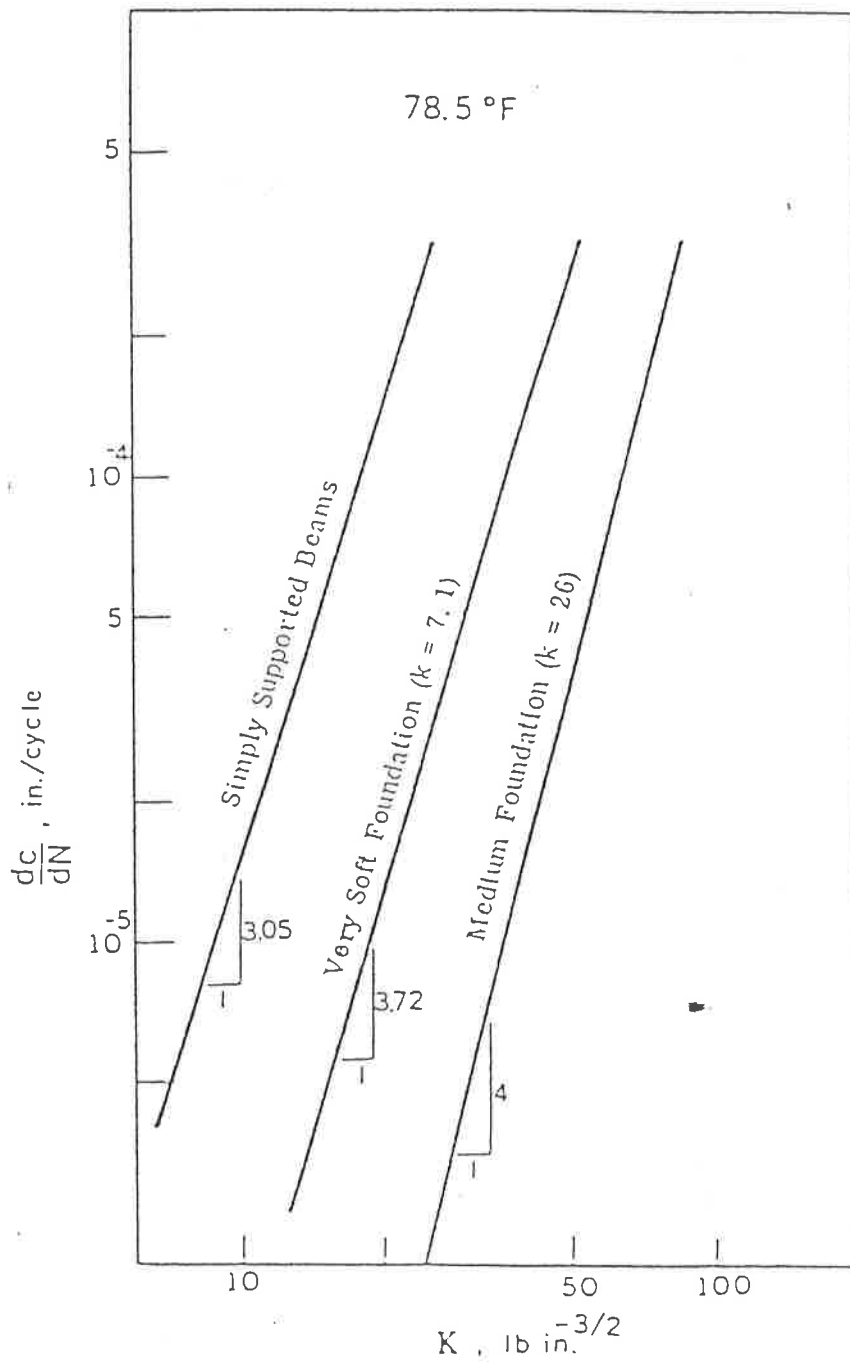


Fig. 6.1 Comparison of Rates of Crack Propagation in Simply Supported Beams and Beams on Elastic Foundation (Majidzadeh, et.al., 1991)

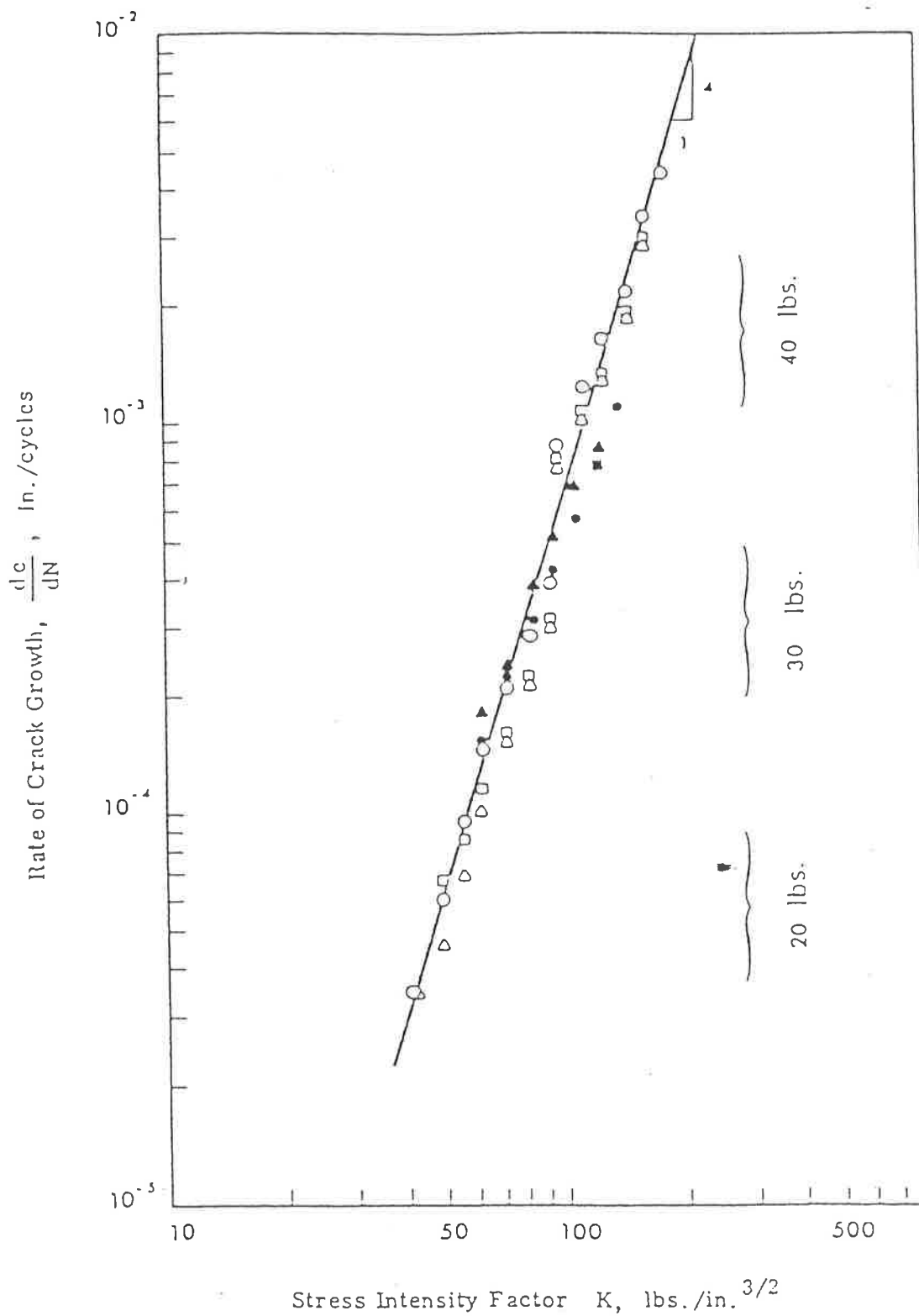


Fig.6.2  $K$  vs  $da/dN$  for Monotonic Loading with Different Load Level (Majidzadeh, et.al., 1991)

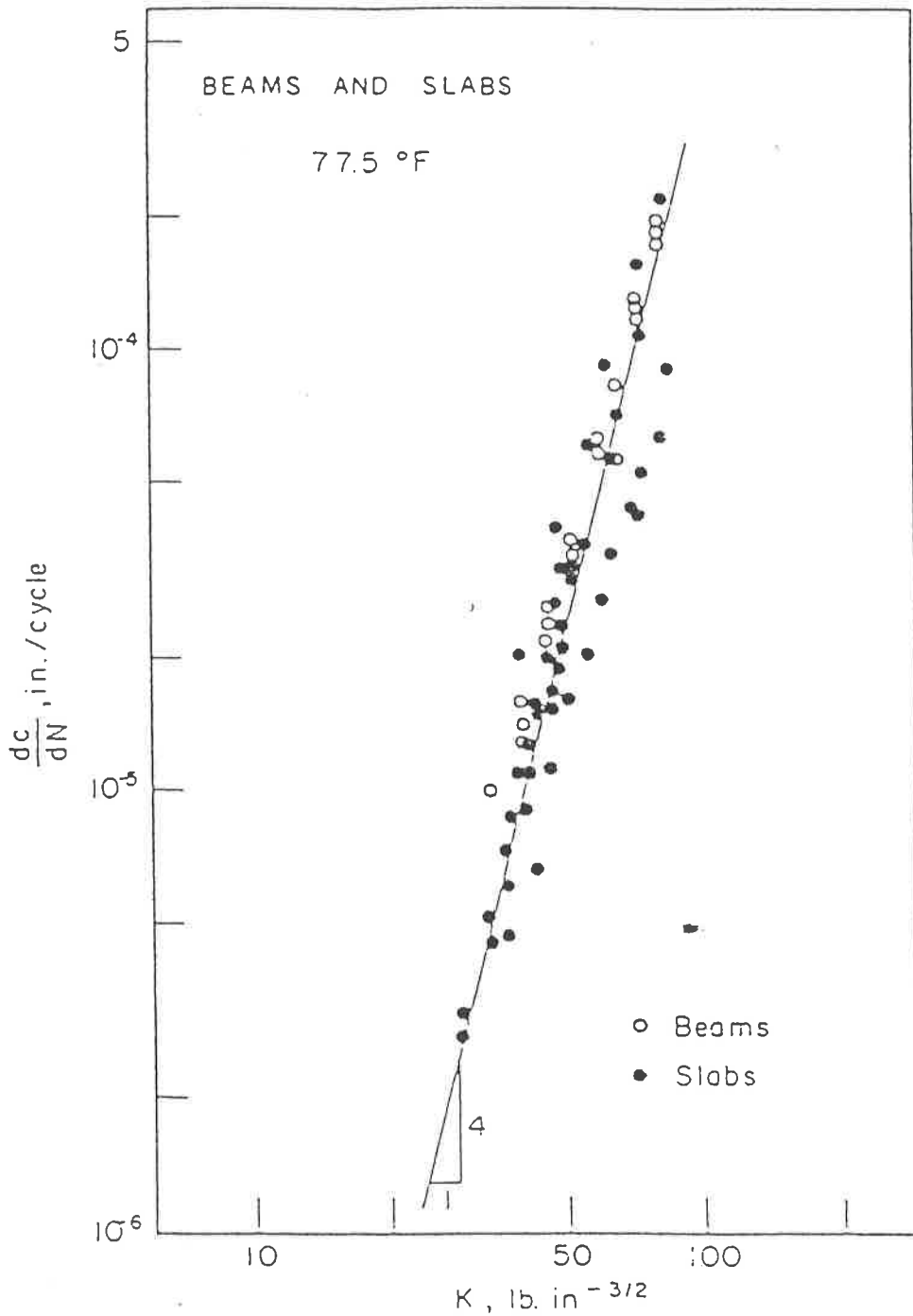


Fig. 6.3 Comparison of Crack Growth Rates for Beams on Elastic Foundations and Slab Test (Majidzadeh, et.al.,1991)

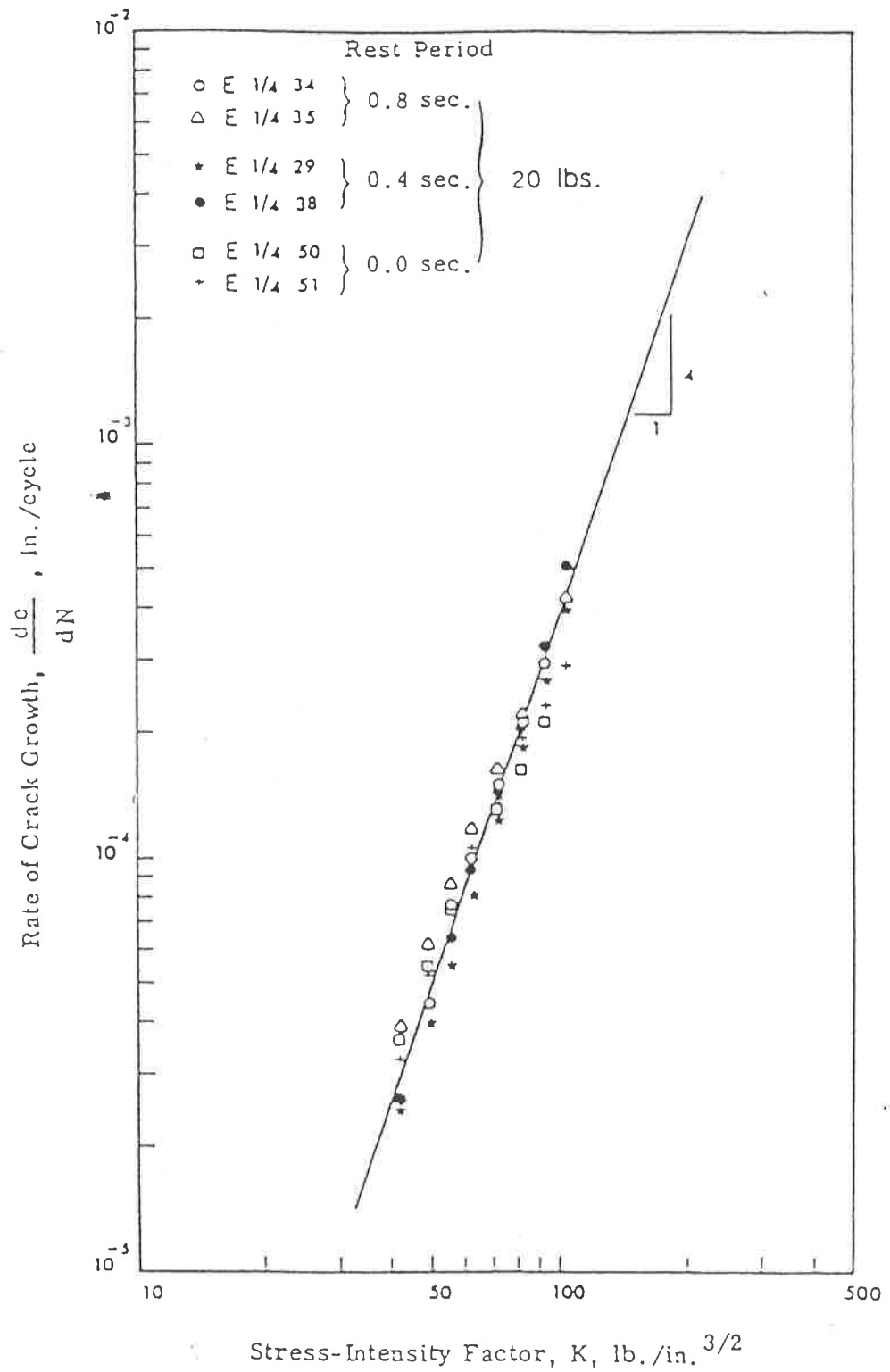


Fig. 6.4  $K$  vs  $da/dN$  for 20 lbs Loading with Different Rest Period (Majidzadeh, et.al., 1991)

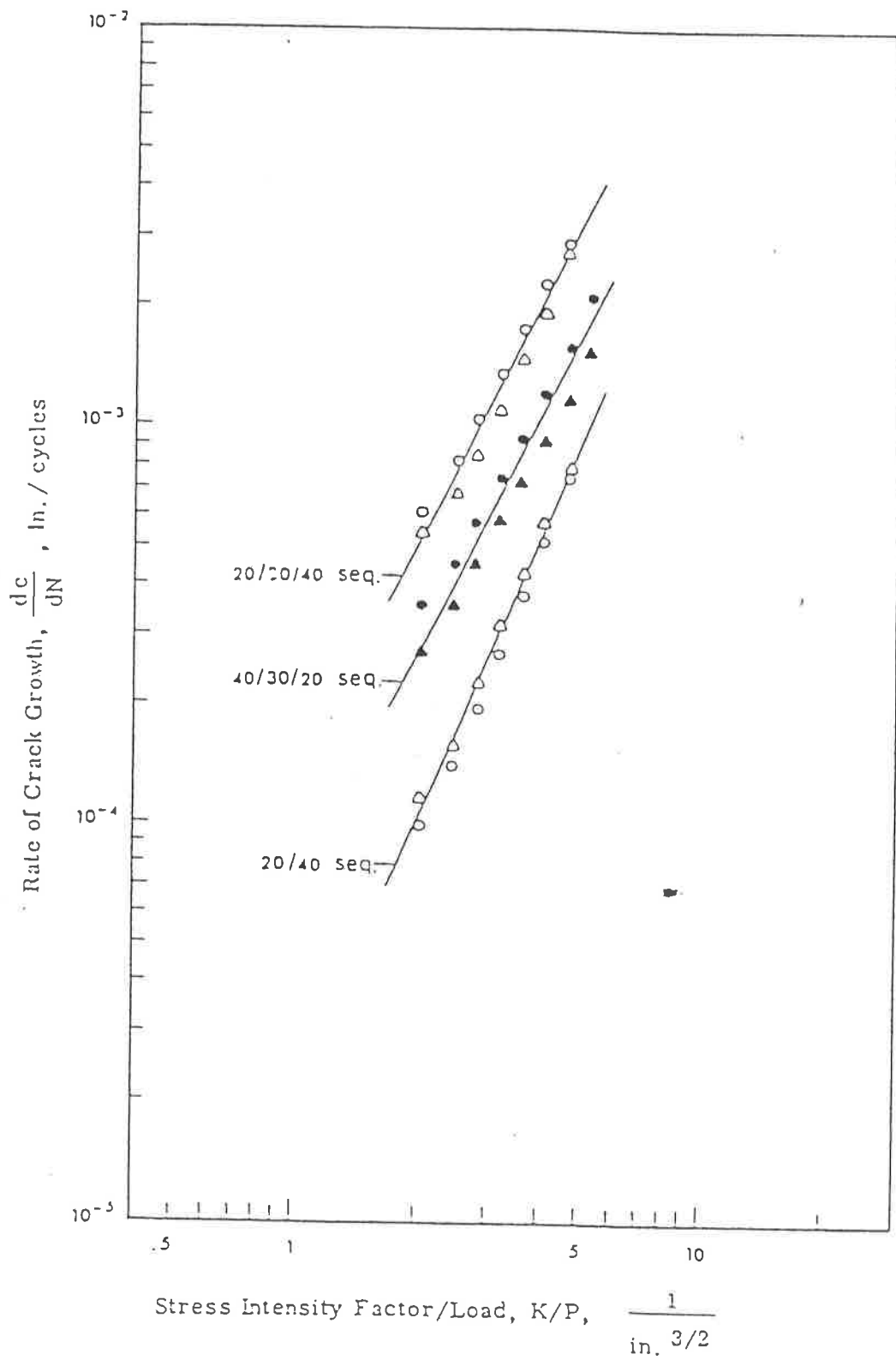


Fig. 6.5 Effect of Sequential Loads on  $da/dN$  vs  $K/P$  (Majidzadeh, et.al., 1991)

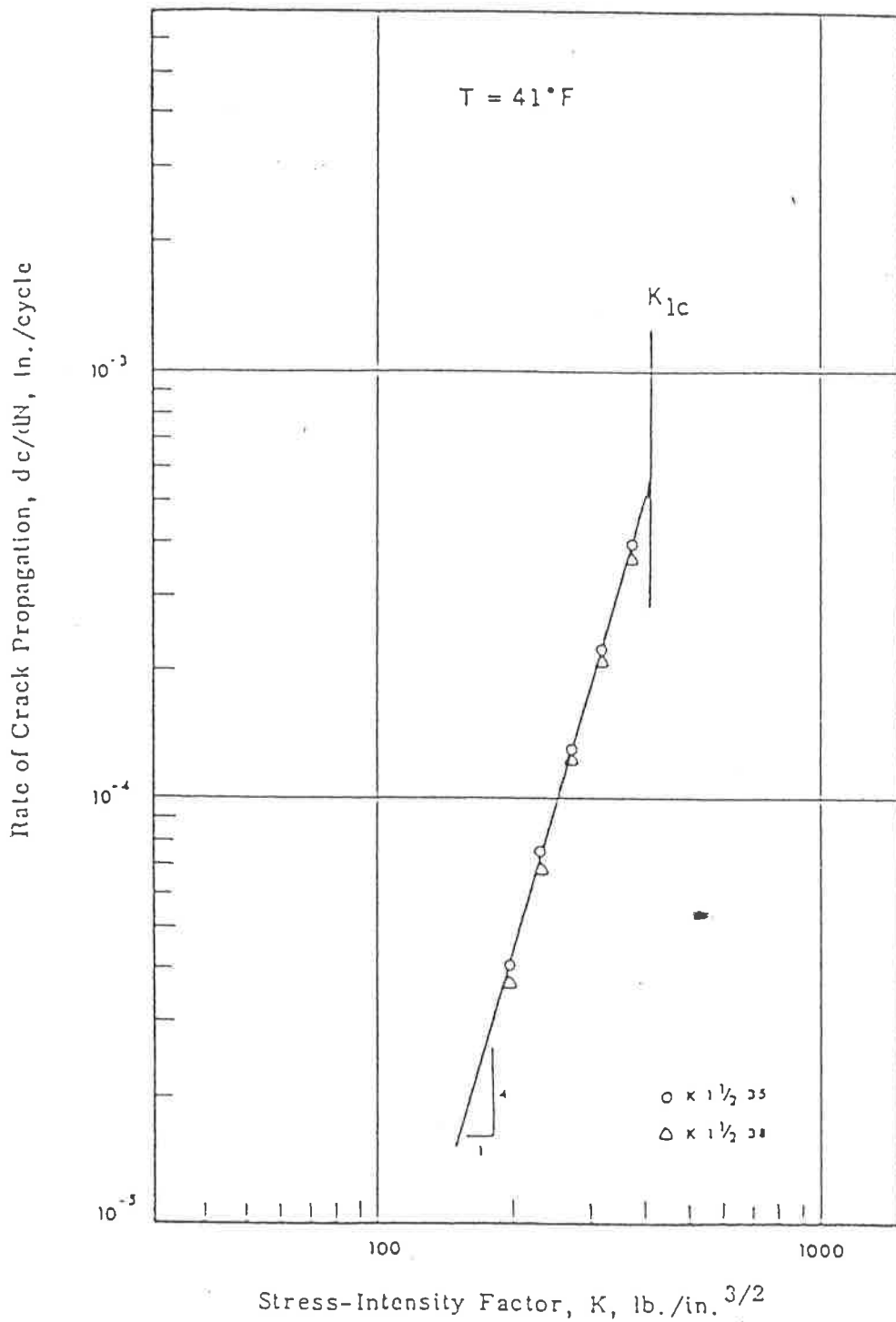


Fig. 6.6  $da/dN$  vs  $K$  for Temperature of 41°F  
(Majidzadeh, et.al., 1991)

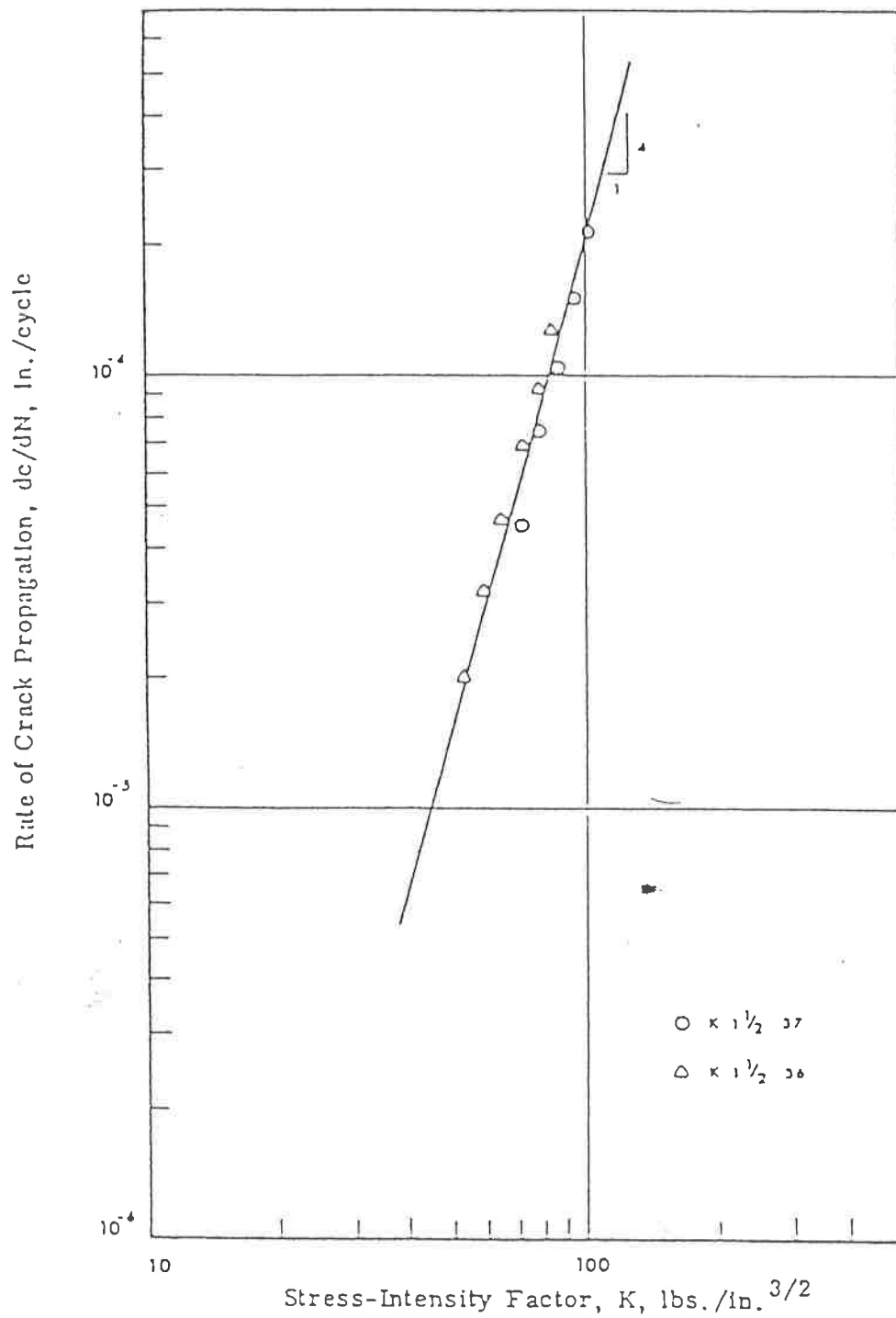


Fig. 6.7  $da/dN$  vs  $K$  for Temperature of 90°F  
 (Majidzadeh, et.al., 1991)

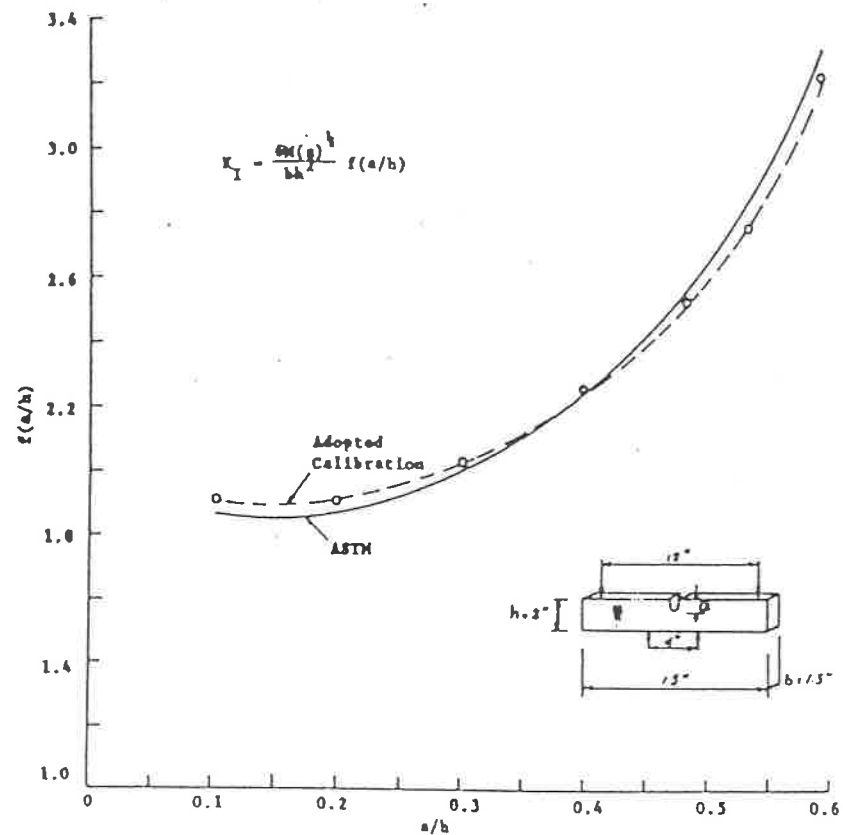


Fig. 7.1  $K_I$  Calibration for Single-edge Notch Beam (Bending) (Monismith, et.al., 1971)

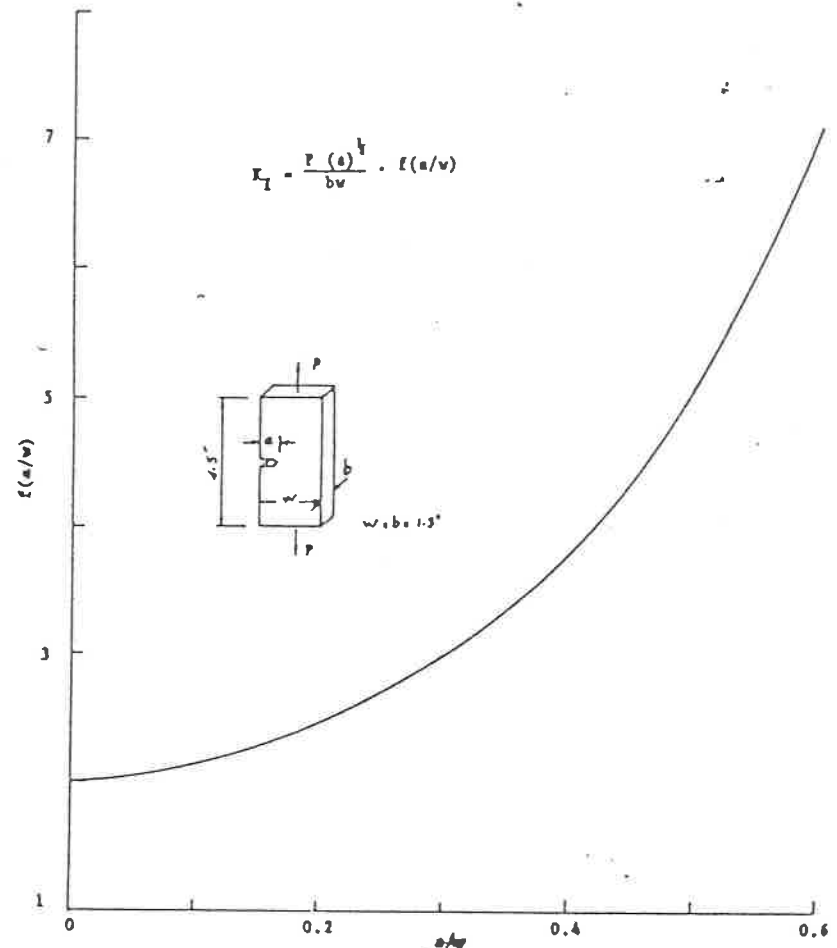


Fig. 7.2  $K_I$  Calibration for Single Edge Notch for Tension (Monismith, et.al., 1971)



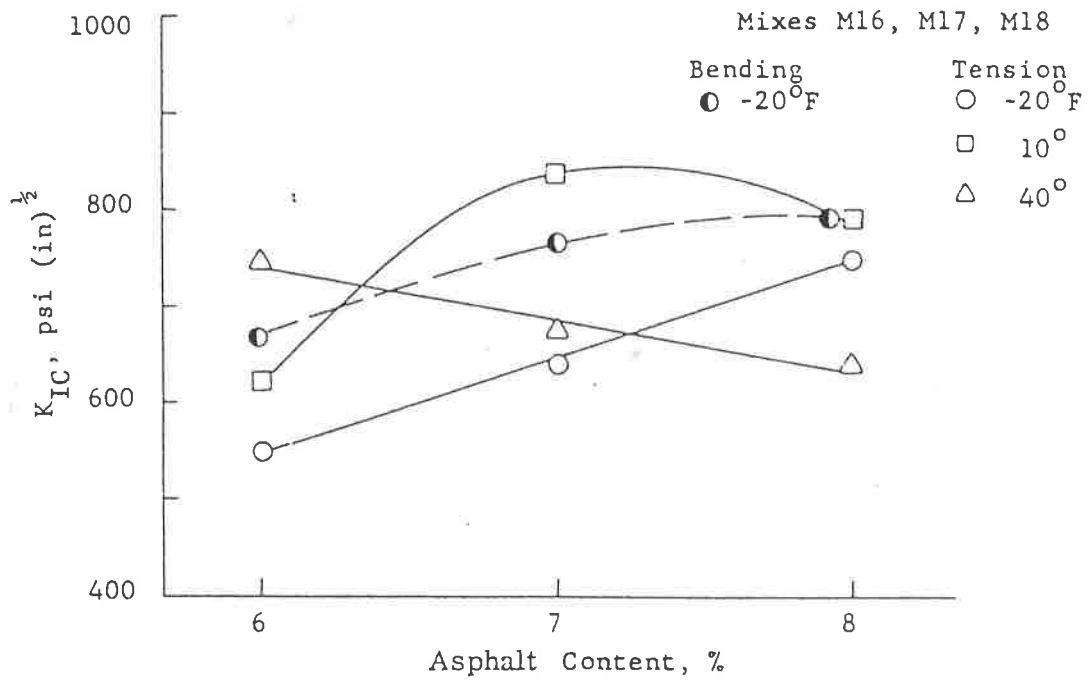


Fig. 7.3 Influence of Asphalt Content on  $K_{IC}$  (Monismith, et.al., 1971)

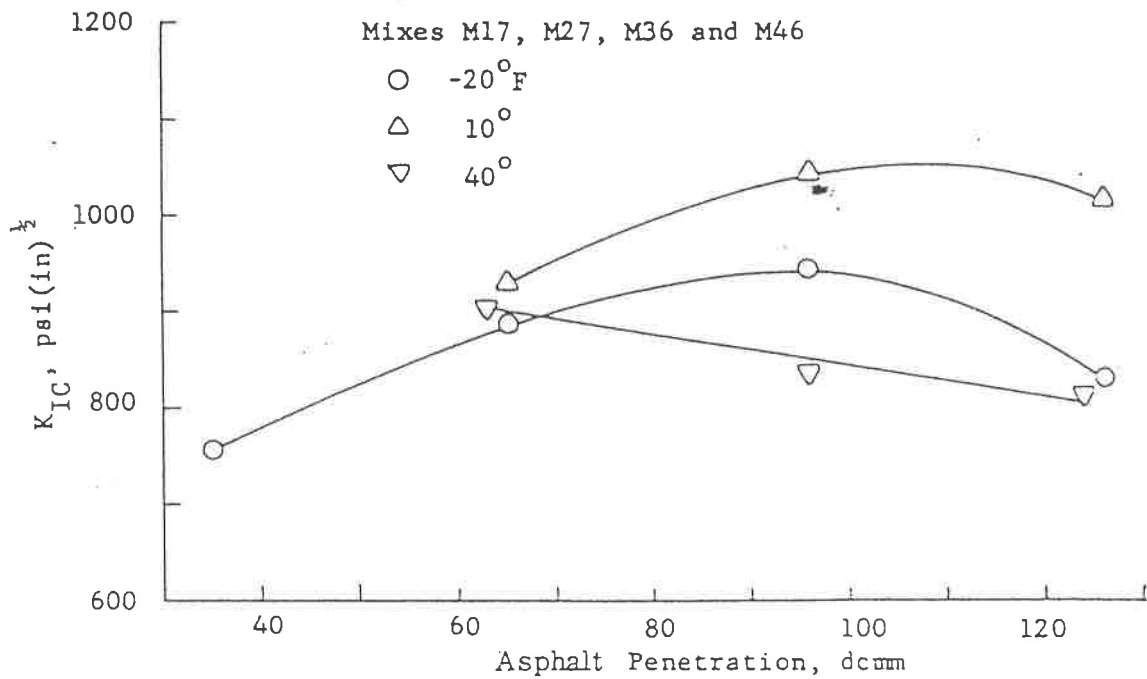


Fig. 7.4  $K_{IC}$  vs Asphalt Penetration on Bending Test (Monismith, et.al., 1971)

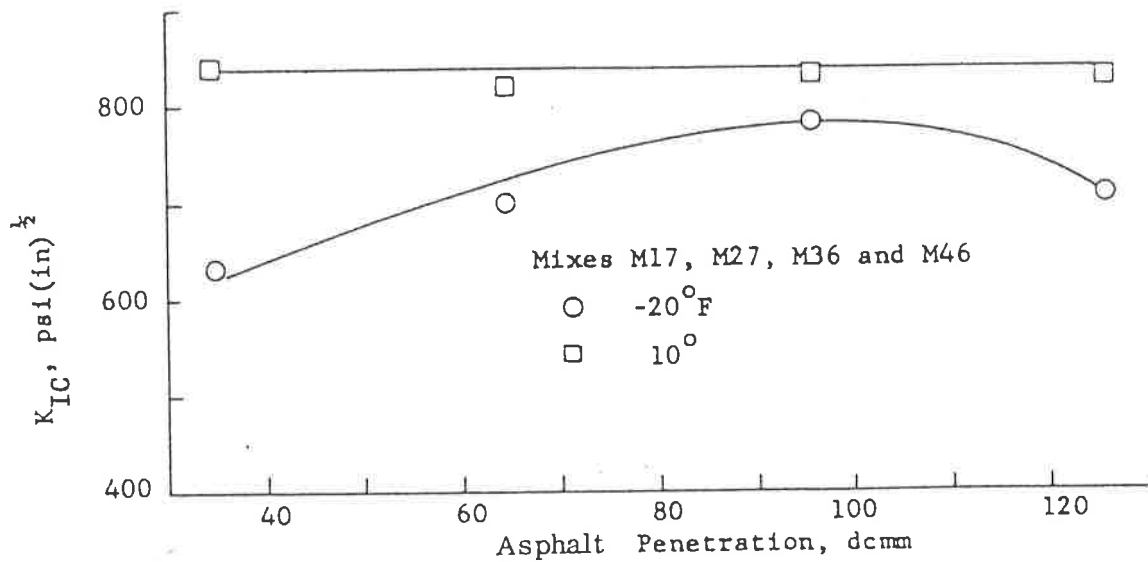


Fig. 7.5  $K_{IC}$  vs Asphalt Penetration for Tension Specimen (Monismith, et. al., 1971)

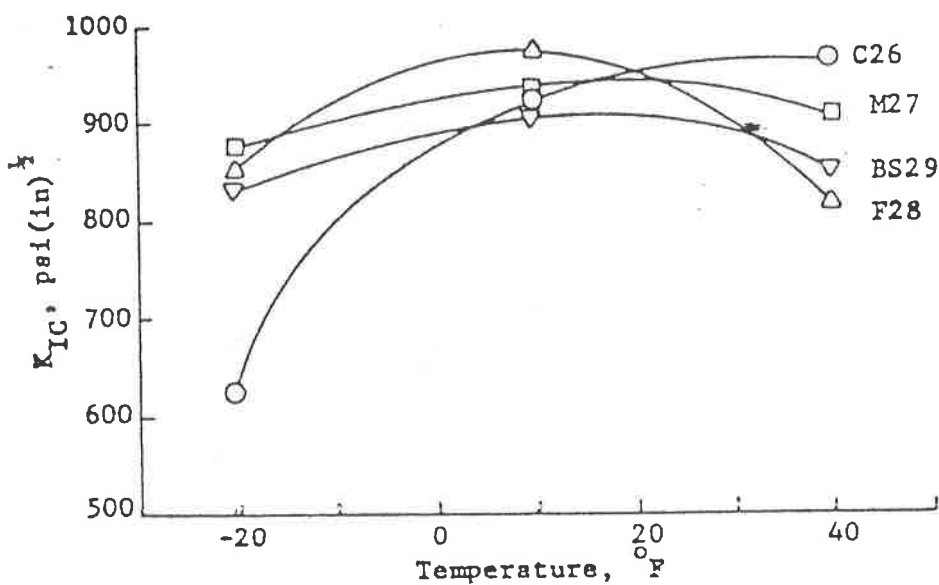


Fig. 7.6 Influence of Aggregate Gradation on Fracture Toughness for Bending Test (Monismith, et.al., 1971)

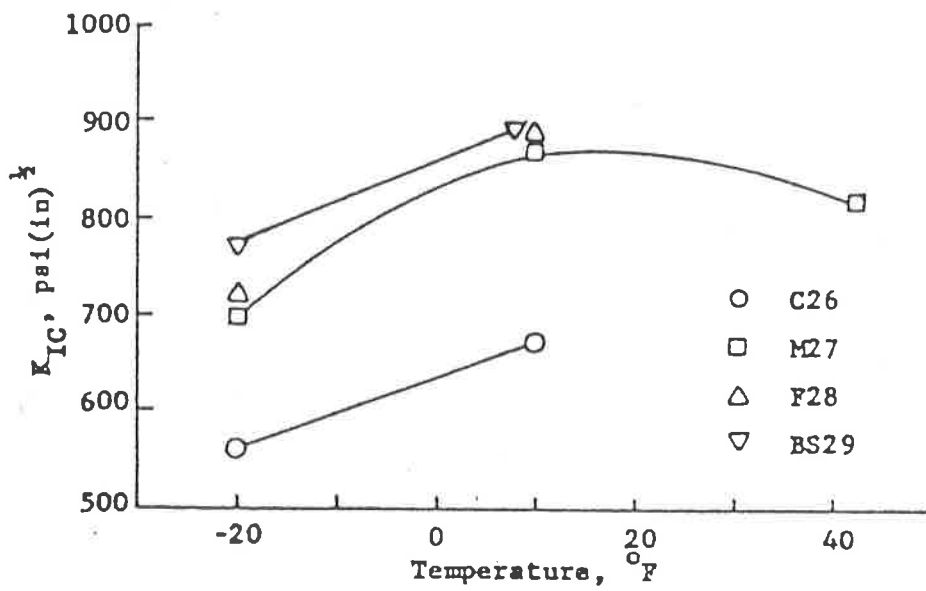


Fig. 7.7 Influence of Aggregate Gradation on Fracture Toughness for Tension Test (Monismith, et. al., 1971)

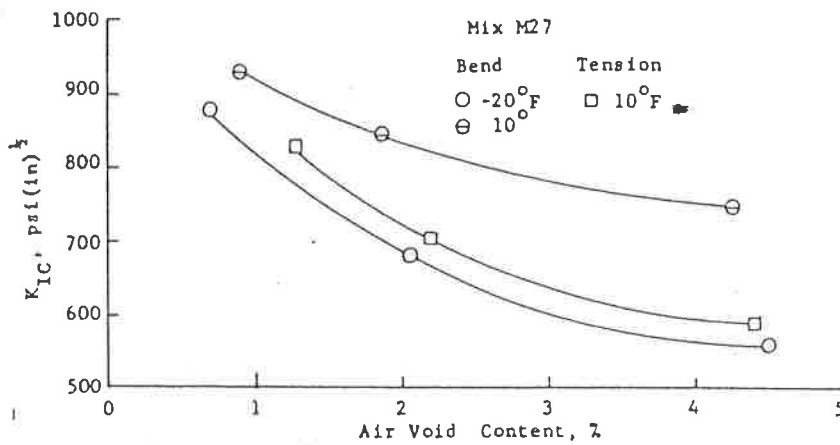


Fig. 7.8 K<sub>IC</sub> vs Air Voids for Mix M 27 (Monismith, et.al., 1971)

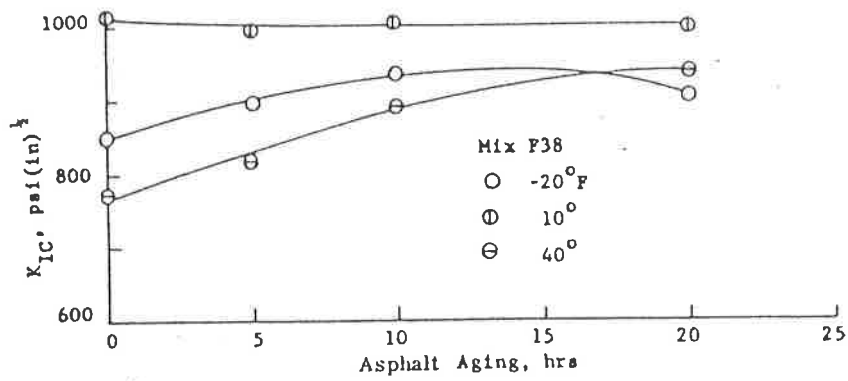


Fig.7.9 Influence of Asphalt Ageing on Fracture Toughness for Bending Test (Monismith, et.al., 1971)

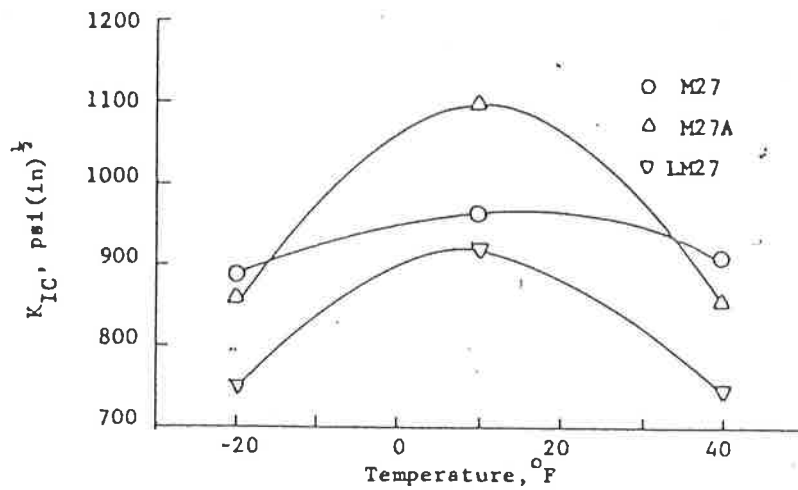


Fig.7.10 Influence of Mix Ageing and Aggregate Type on Fracture Toughness for Bending Test (Monismith, et.al., 1971)

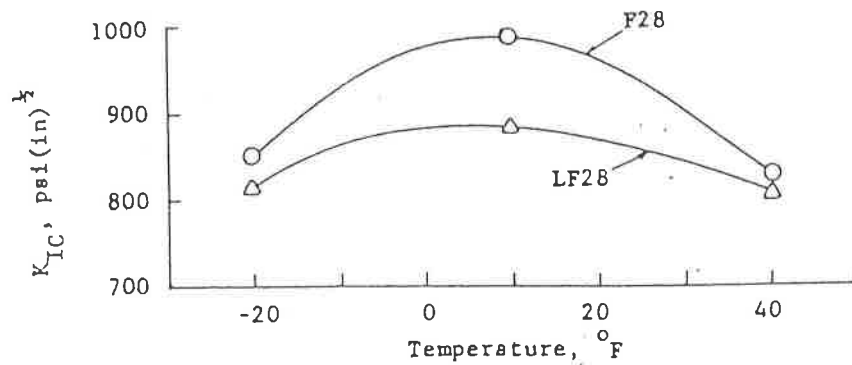


Fig.7.11 Influence of Mineral Filler on Fracture Toughness for Bending Test (Monismith, et.al., 1971)

Table 7.1. Asphalt Mixture Designation in Monismith's Laboratory Tests (monismith, et.al.,1971)

Mixture Designation	Aggregate Gradation	Asphalt Type	Asphalt Content, %	Aggregate Type	Type of Mineral Filler
M16	Medium	40 - 50	6	Granite	Granite
M17	Medium	40 - 50	7	Granite	Granite
M18	Medium	40 - 50	8	Granite	Granite
M27	Medium	60 - 70	7	Granite	Granite
LM27	Medium	60 - 70	7	Limestone	Limestone
M36	Medium	85 - 100	6	Granite	Granite
M46	Medium	120 - 150	6	Granite	Granite
C26	Coarse	60 - 70	6	Granite	Granite
F28	Fine	60 - 70	8	Granite	Granite
LF28	Fine	60 - 70	8	Granite	Limestone
BS29	BS-594	60 - 70	9	Granite	Granite
M28	Medium	60 - 70	8	Granite	Granite
F38	Fine	85 - 100	8	Granite	Granite

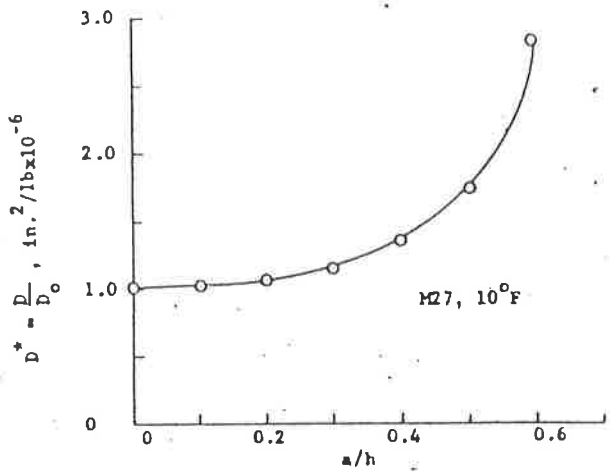


Fig.8.1 Normalized Deflection Compliance as a Function of a/h (Monismith, et. al., 1971)

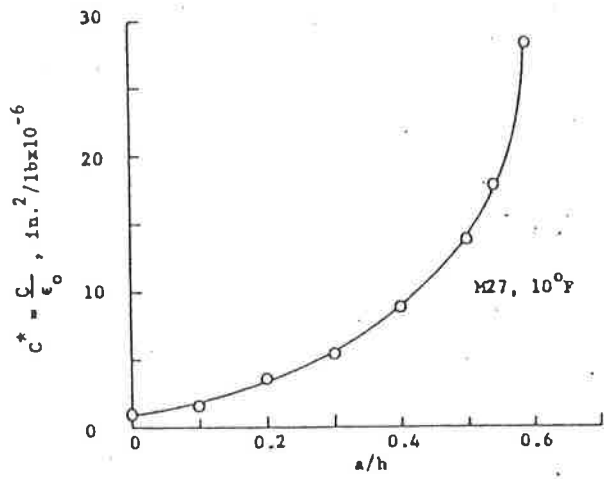


Fig.8.2 Normalized Crack Compliance as a Function of a/h (Monismith, et. al., 1971)

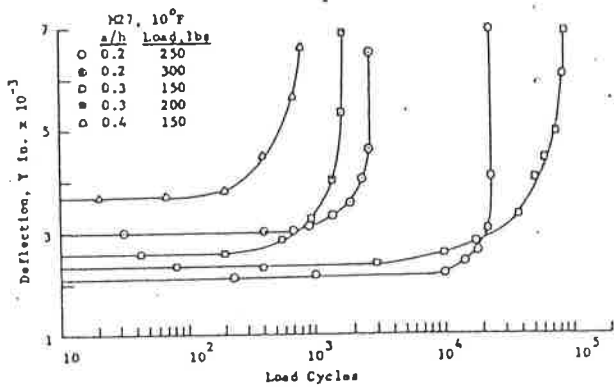


Fig. 8.3a Deflection vs N at 10^0 F (Monismith, et. al., 1971)

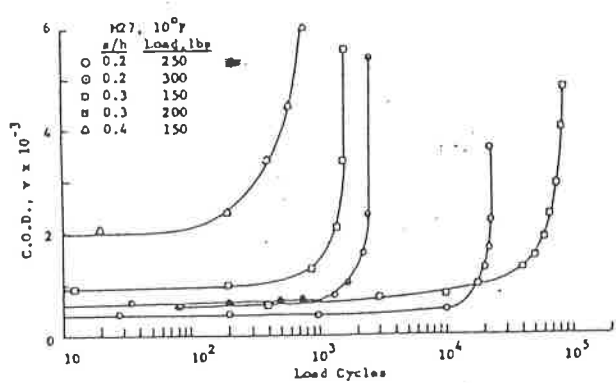


Fig.8.3b CTOD vs N at 10^0 F (Monismith, et. al., 1971)

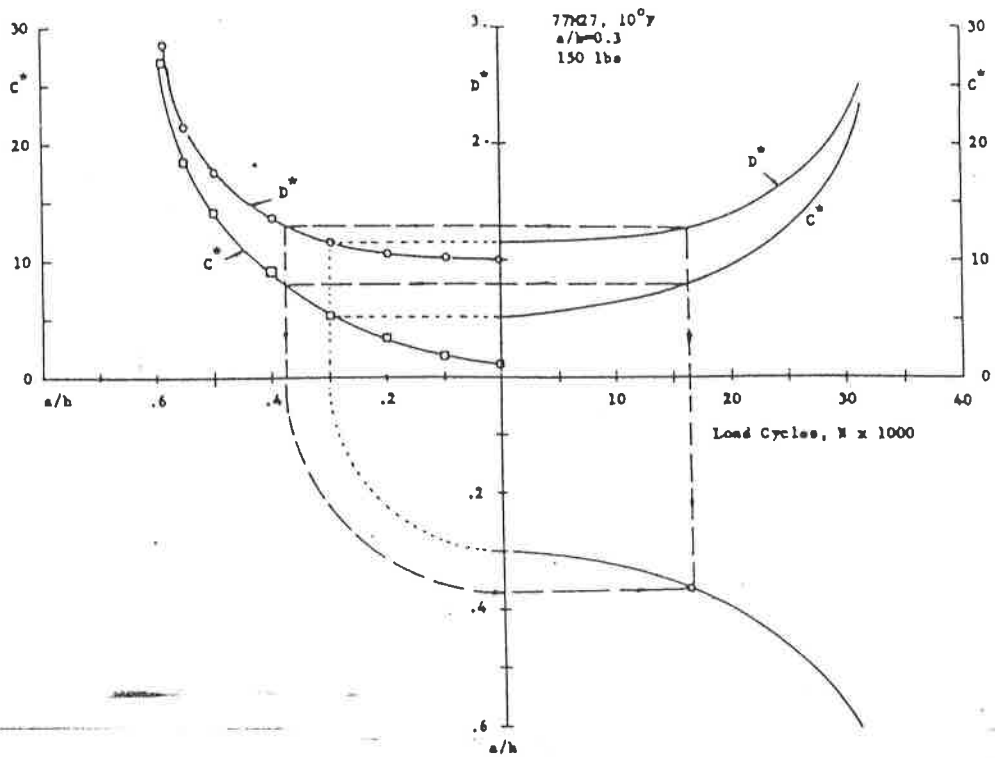


Fig. 8.4 Relationship of Compliance, N, and a/h from Mix M27 at 10°F (Monismith, et.al.,1971)

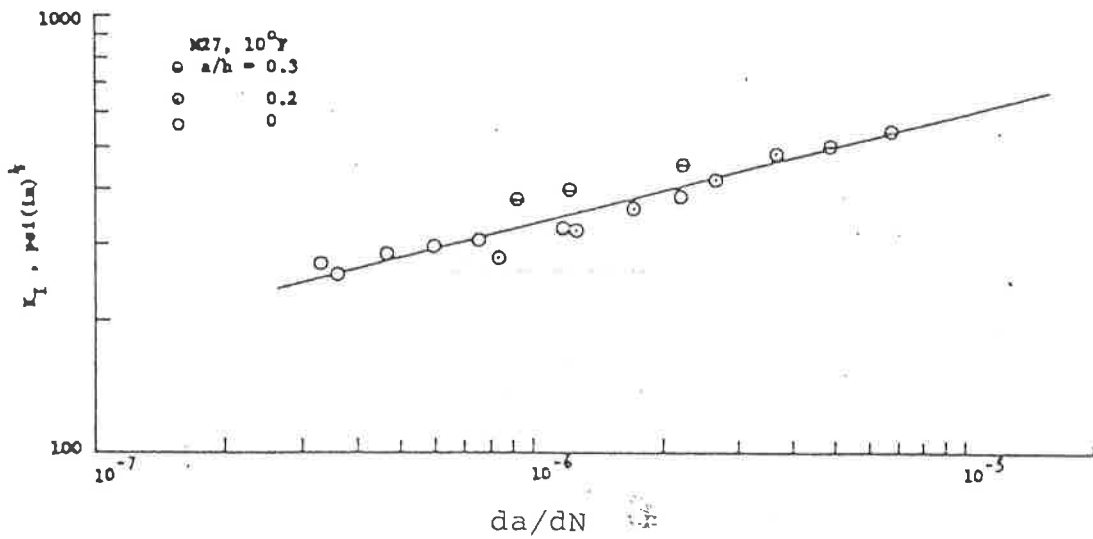


Fig.8.5 Fatigue Growth Rate as a Function of  $K_I$  for Mix M27, at 10°F (Monismith, et.al.,1971)